A super-enhancer actuated by heterodimerization of a specific YAP1 isoform, YAP1-2α, with TAZ endows cancer stemness and drug resistance

Takuya Ooki,[1] Takeru Hayashi,[1] Yui Yamamoto,[1] and Masanori Hatakeyama[1,2,3]*

[1]Laboratory of Microbial Carcinogenesis, Institute of Microbial Chemistry, Microbial Chemistry Research Foundation, Tokyo 141-0021, Japan

[2]Center of Infection-associated Cancer, Institute for Genetic Medicine, Hokkaido University, Sapporo 060-0815, Japan

[3]Lead contact

***Correspondence: mhata@m.u-tokyo.ac.jp**

SUMMARY

Molecular targeted drugs are frequently used in precision cancer therapies. However, the prolonged administration of these agents can result in drug resistance. Cancer cells exhibiting defects in homologous recombination are particularly susceptible to genotoxic stress, such as that induced by PARP inhibitors (PARPi), resulting in synthetic lethality. Here, we show that sustained treatment of such cancer cells with PARPi selectively upregulates YAP1-2α, a minor isoform of YAP1. Elevated YAP1-2α heterodimerizes with TAZ to induce liquid-liquid phase separation (LLPS) in the nucleus. This LLPS-driven process generates nuclear condensates that activate a super-enhancer comprising YAP1-2α, TAZ, TEAD, and BRD4. The super-enhancer reconfigures transcriptional networks to enhance cancer stem-like malignant properties, thereby potentiating cell resilience and augmenting cell resistance to adverse conditions, including precision cancer therapies. Our study reveals the presence of a super-enhancer that promotes malignant tumor progression. Targeting the YAP1-2α/TAZ-induced super-enhancer is a promising strategy for overcoming resistance to anticancer modalities.

INTRODUCTION

Molecular targeted therapies selectively attack cancer cells, disrupting pathways essential for tumor growth and survival while reducing the severe side effects.[1] Imatinib, a small-molecule kinase inhibitor targeting BCR-ABL in chronic myelogenous leukemia (CML), is an early success in this field.[2] Other kinase inhibitors have also shown improved responses in cancer cells with driver mutations in their respective kinases.[3] Beyond kinase inhibitors, monoclonal antibodies such as those targeting the EGF receptor and HER2 have been successfully applied to treat specific cancers.[4] Treatment of cancers with inactivating mutations in genes essential for homologous recombination (HR) such as *BRCA1* and *BRCA2* (collectively referred to as *BRCA*-deficient cancers) induces synthetic lethality with poly ADP-ribose polymerase inhibitor (PARPi) through excessive DNA double-strand break (DSB) induction.[5]

Molecular targeted therapies have revolutionized cancer treatment but face challenges like drug resistance. Cancer cells can develop treatment drug-specific resistance through back mutations or second-site mutations in target molecules, which impair drug binding.[6] Other mechanisms include increased drug degradation or efflux and activation of alternative pathways bypassing targeted signaling.[7] Additionally, as cancer cells acquire cancer stem-like properties, they resist adverse conditions caused by anticancer modalities.[8] The acquisition of cancer stem-like properties is key to malignant progression, with recent studies showing that differentiated cancer cells can revert to a stem-like state,[9]

indicating that cancer stemness is a dynamic state rather than a fixed cell population.[10-12] Epithelial-to-mesenchymal transition (EMT) enhances cell stemness, increasing invasion, metastasis, and resistance to treatments.[9,13-15] Enhancing cancer stem-like properties may require dynamic transcriptional network restructuring, bolstering cancer cell resilience.

A super-enhancer is a cluster of enhancers that contact target promoters via chromatin looping during transcription, with high levels of transcription factors, co-activators, and epigenetic modifiers. Master transcription factors co-occupy the super-enhancer, forming a core regulatory circuitry to manage cell transcriptional programs.[16] Liquid-liquid phase separation (LLPS)-mediated condensation of transcription factors and co-activators is one of the significant processes in assembling the transcription machinery to activate super-enhancers.[17,18] Cancer cells can exploit super-enhancers to perturb physiological transcriptional networks, enhancing malignant traits by aberrantly activating mitogenic signaling, anti-apoptotic machinery, migration/metastasis processes, DNA repair systems, and creating tumor-favorable microenvironments, including cold immune conditions.[19-24] Consequently, cancer cells comprehensively reinforce resistance to various anticancer therapies.[25]

The tumor-suppressive Hippo signal-regulated transcriptional coactivators Yes-associated protein-1 (YAP1) and its paralog TAZ (WW domain containing transcription regulator 1, or WWTR1) play a crucial role in cancer initiation, growth, and progression across most solid

tumors.[26] Lacking a DNA-binding domain, YAP1 and TAZ activate downstream transcription by interacting with sequence-specific transcription factors, mainly the TEAD family of transcription factors (TEAD1-4).[27,28] They integrate mechanical, metabolic, and cell-density signals to regulate cell proliferation and differentiation during development and neoplastic progression by activating classical enhancers and super-enhancers.[29,30] Elevated YAP1 and TAZ expression promotes stemness and inhibits differentiation, increasing organ size and developmental abnormalities.[31] YAP1 and TAZ also contribute to drug resistance in various cancers.[32] YAP1 and TAZ-mediated transcriptional programs intersect with the KRAS-ERK MAPK pathway to share target genes.[33,34] Thus, high YAP1 levels confer resistance to RAF and MEK inhibitors in many cancers.[35] Additionally, YAP1 and TAZ enhance cancer cell stemness by inducing epithelial-to-mesenchymal transition (EMT) via TEAD-dependent transactivation of EMT-inducing regulators such as ZEB1 and Slug.[36] While YAP and TAZ cooperate in controlling gene expression,[37] their binding sites are not always identical/overlapping,[38] indicating that YAP1 and TAZ may act in a distinct subset of enhancers/super-enhancers. Consistently, the ability of YAP1 and TAZ to undergo LLPS varies significantly; TAZ induces LLPS via homodimerization through its Leucine zipper protein-protein binding motif in the coiled-coil domain,[39] whereas YAP1 has been reported not to readily induce LLPS due to its inability to undergo homodimerization via the coiled-coil domain.[40] These findings suggest that YAP1-driven super-

enhancers, which may not use LLPS, and TAZ-driven super-enhancers, act independently within cells.

We previously discovered that among the eight predominant human YAP1 isoforms, which are generated by differential splicing of *YAP1* pre-mRNA, only YAP1-1α and YAP1-2α, which are typically minor in somatic cells, contain the functional Leucine zipper in the coiled-coil domain. These specific YAP1 isoforms cannot homodimerize but heterodimerize with TAZ through their Leucine zippers.[40] The present study found that YAP1-2α becomes upregulated in *BRCA*-deficient cancer cells under genotoxic stress, such as prolonged treatment with PARPi or Cisplatin. Consequently, the YAP1-2α/TEAD complex associates with the TAZ/TEAD complex via the Leucine zippers, leading to the induction of LLPS that activates the YAP1-2α/TAZ/TEAD super-enhancer. This super-enhancer establishes a transcriptional network that increases cancer stem-like properties, conferring resistance to anticancer modalities, including molecular targeted drugs. Our study connects differential splicing of *YAP1* pre-mRNA and super-enhancers through LLPS, suggesting that inhibiting YAP1-2α could impede cancer progression and help prevent cancer-treatment resistance.

RESULTS

Establishment of PARPi-resistant cells from *BRCA*-deficient cancer cells

To elucidate the mechanism behind *BRCA*-deficient cancers' resistance to PARPi-induced synthetic lethality, we generated PARPi-resistant cells from two human *BRCA1*-mutated cancer cells: MDA-MB-436 triple-negative breast cancer and UWB1.289 serous ovarian cancer (Figure S1A). To assess drug resistance specificity, we exposed parental and PARPi-resistant cells to DNA-damaging agents (Olaparib, Cisplatin) and non-DNA-damaging agents (Paclitaxel, Staurosporine). Results showed that PARPi-resistant cells resisted Cisplatin but not Paclitaxel and Staurosporine, indicating acquired resistance to conventional DNA-damaging agents (Figure S1B, S1C and S1D).

We conducted RNA-sequencing (RNA-seq) analysis on PARPi-resistant cells derived from MDA-MB-436 and UWB1.289 and compared their gene expression profiles to those of parental cells (Figure 1A). Gene ontology and hallmark gene set analyses were performed on 1,132 commonly upregulated genes in the resistant cells. PARPi resistance was linked to increased gene expression in innate immune/inflammatory responses such as SASP and enhanced cytokine/chemokine signaling, likely induced by cGAS-STING signaling from PARPi trapping-induced DNA damage.[41] RNA-seq data also showed elevated expression of genes related to EMT, suggesting dedifferentiation of the resistant cancer cells. This was supported by higher mRNA levels of YAP and TAZ signaling,

KRAS signaling, WNT signaling, anti-ROS signaling, and anti-apoptotic signaling. Additionally, genes associated with cell stemness were more highly expressed in PARPi-resistant cells than in parental cells (Figure S1E). The elevated expression of genes involved in recognizing and repairing DNA double-strand breaks, including error-prone microhomology-mediated end-joining (MMEJ) and single-strand annealing (SSA) (Figure 1A), may explain the increased resistance of PARPi-resistant *BRCA*-deficient cancer cells to conventional DNA-damaging agents.

RNA-seq analysis also indicates that PARPi resistance in *BRCA*-deficient cancer cells stems from extensive transcriptional network restructuring that affects the expression of genes involved in various biological processes rather than a change in a small set of genes. To explore this, we examined YAP1 and TAZ transcriptional co-activators, as genes regulated by the TEAD transcription factors (TEAD1-4), the primary targets of YAP and TAZ, were significantly elevated in PARPi-resistant cells (Figure 1B). YAP1 has complex mRNA splicing isoforms, with human cells expressing eight isoforms (Figure S1F).[42] The presence or absence of exon 4, encoding the second WW domain (WW2), classifies YAP1 into YAP1-1 (one WW domain) and YAP1-2 (two WW domains). The WW domain binds proline-containing sequences like PPxY.[43] There are four additional pre-mRNA splicing variants for both *YAP1-1* and *YAP1-2* species. *YAP1-1γ* and *YAP1-2γ* mRNAs contain a shorter exon 5 (exon 5.1, lacking the β-segment) and exon 6. *YAP1-1δ* and *YAP1-2δ* mRNAs feature

a more extended exon 5 (exon 5.2, including the β-segment) and exon 6 (encoding the γ-segment). *YAP1-1β* and *YAP1-2β* mRNAs have exon 5.2 but lack exon 6, while *YAP1-1α* and *YAP1-2α* mRNAs possess exon 5.1 but lack exon 6 (Figure S1F). Among these, only *YAP1-1α mRNA*-derived YAP1-1α and *YAP1-2α* mRNA-derived YAP1-2α splicing isoforms have a functional Leucine zipper in the coiled-coil domain. To examine *YAP1* mRNA splicing patterns in *BRCA*-deficient cancer cells before and after acquiring PARPi resistance, we used RT-PCR to assess exon 6 inclusion or exclusion. We found that *YAP1* splicing variants including exon 6 were predominant in parental cells, whereas variants lacking exon 6 were prevalent in PARPi-resistant cells (Figure 1C). Further splicing variant analysis using RNA-seq data revealed that *YAP1-1* mRNA expression was substantially lower than *YAP1-2* mRNA in both parental and PARPi-resistant cells. In addition, *YAP1-2γ* mRNA was the predominant *YAP1-2* splicing variant in parental cells (Figure S1G). However, in PARPi-resistant cells, *YAP1-2α* mRNA levels notably increased, while *YAP1-2β*, *YAP1-2γ*, and *YAP1-2δ* mRNA levels significantly decreased (Figures 1D, 1E and S1G). TCGA database analysis also showed that most human cancers predominantly express *YAP1-2γ* mRNA containing exons 5.2 and 6 (Figure S1H). Thus, the predominant expression of YAP1-2α mRNA, a minor YAP1 splicing isoform in most cancer and normal cells, is a distinctive feature of PARPi-resistant cancer cells.

PARPi-resistant MDA-MB-436 and UBW1.289 cancer cells also

resisted Cisplatin (Figures S1C and S1D). Similarly, Cisplatin-resistant UWB1.289 cells exhibited altered *YAP1* pre-mRNA splicing patterns (Figure 1F). The resistance of cancer cells to DNA-damaging agents like PARPi and Cisplatin correlated with a shift in *YAP1* pre-mRNA splicing from the YAP1-2γ-dominant to the YAP1-2α-dominant pattern. To determine if the YAP1-2α isoform contributes to this resistance, MDA-MB-436 and UWB1.289 cells stably expressing each of the YAP1-2 splicing isoforms were created. Upon treatment with Olaparib or Cisplatin, only cells ectopically expressing YAP1-2α showed resistance (Figure 1G). These results indicate that increased expression of the YAP1-2α isoform is linked to cancer cell resistance to genotoxic stress, such as PARPi or Cisplatin.

YAP1-2α induces LLPS in a splicing variation-dependent manner

To clarify the mechanism by which elevated levels of YAP1-2α contribute to drug resistance in cancer cells, we investigated the subcellular distribution of YAP1 in both parental and PARPi-resistant cells. Immunofluorescence staining of the parental cells, which predominantly expressed YAP1-2γ, revealed that YAP1 was broadly and uniformly distributed throughout the nucleus, except for the nucleoli. In contrast, in the PARPi-resistant cells that primarily expressed YAP1-2α, YAP1 immunofluorescence staining demonstrated the formation of punctate structures within the nucleus (Figures 2A and S2A). Administration of 1,6-

hexanediol (Hex), an agent that disrupts liquid-like condensates without affecting solid aggregates, to PARPi-resistant cells eliminated puncta formation. YAP1-2α-associated puncta formation was also observed in Cisplatin-resistant UWB1.289 cells (Figure S2B). We also generated *YAP1*-knockout (KO) UWB1.289 cells utilizing the CRISPR-Cas9 system. Immunoblot analysis confirmed the absence of endogenous YAP1-1 and YAP1-2 isoforms in the *YAP1*-KO cells (Figure 2B, lane 2). These *YAP1*-KO cells were subsequently transfected with an expression vector for one of the four YAP1-2 splicing isoforms fused with mVenus. The expression levels of the mVenus-fused YAP1-2 splicing isoforms were comparable (Figure 2B, lanes 3-6). We found nuclear puncta formation only in cells expressing mVenus-fused YAP1-2α (Figures 2C, 2D, S2C and S2D). To exclude the possibility that the puncta formation was due to the overexpression of mVenus-fused YAP1-2α, we also established *YAP1*-KO UWB1.289 cells reconstituted with HA-tagged YAP1-2α or YAP1-2γ at levels comparable to that of endogenous YAP1. Immunofluorescence analysis using an anti-YAP1 antibody revealed that nuclear YAP1 puncta were present in YAP1-2α-reconstituted cells but absent in YAP1-2γ-reconstituted cells (Figure 2E). This finding indicates that YAP1-2α induces LLPS-mediated puncta formation in the nucleus. To further elucidate the membrane-less, liquid-like properties of the nuclear puncta induced by YAP1-2α, we conducted time-lapse imaging experiment and FRAP analysis in *YAP1*-KO UWB1.289 cells transfected with mVenus-fused YAP1-2α. YAP1-2α was demonstrated to be responsible for

membrane-less puncta formation (Figures 2F-2I and S2E-S2H). Based on these observations, we concluded that YAP1-2α is the only YAP1-2 splicing isoform capable of inducing LLPS in the nucleus.

LLPS is induced by YAP1-2α/TAZ complex formation

A previous study showed that the Leucine zipper in the coiled-coil region of YAP1-2α interacts with the Leucine zipper in TAZ's coiled-coil domain, forming a YAP1/TAZ heterodimer.[40] To determine if the Leucine zipper structure of YAP1-2α is crucial for LLPS-induced puncta formation, we created a YAP1-2α Leucine zipper mutant (LZM) by substituting the conserved Leucine residues with alanine, disrupting its structure. This disruption significantly reduced TEAD reporter activation by YAP1-2α (Figure S3A). Expressing mVenus-fused YAP1-2α(LZM) in YAP1-KO UWB1.289 or MDA-MB-436 cells markedly decreased puncta formation (Figures 3A, S3B and S3C). A proximity ligation assay (PLA) examined YAP1-2α and TAZ heterodimerization, revealing the YAP1-2α/TAZ complex in nuclear YAP1 puncta (Figure 3B). TAZ also formed a heterodimer with YAP1-2α(S94A) but not with YAP1-2α(LZM), YAP1-2α(LZM|S94A), or YAP1-2γ in the nucleus (Figure S3D, upper). As expected, YAP1-2α, YAP1-2α(LZM), and YAP1-2γ interacted with TEAD, while YAP1-2α(S94A) and YAP1-2α(LZM|S94A) did not (Figure S3D, lower). Moreover, YAP1-2α-induced LLPS puncta were eliminated by knocking out endogenous TAZ (Figures 3C and S3E) or by siRNA-

mediated inhibition of TAZ expression (Figure S3F), confirming the essential role of TAZ in YAP1-2α-mediated LLPS induction.

To determine if TEAD (TEAD1-4), the critical YAP1-2α and TAZ partners, is necessary for LLPS-mediated nuclear puncta formation, we expressed mVenus-fused YAP1-2α variants (wild-type, LZM, S94A) and mVenus-fused YAP1-2γ in UWB1.289 cells. PLA (Figures 3D and 3E) and immunofluorescence staining (Figure S3G) indicated a physical interaction between TEAD and wild-type YAP1-2α in nuclear puncta but not the LZM or S94A mutant. Moreover, K-975, a selective inhibitor of the interaction between TEAD and YAP1 or TAZ.[44] eliminated LLPS puncta induced by YAP1-2α (Figures 3F and S3H). Thus, YAP1-2α-induced nuclear condensates contained YAP1-2α, TAZ, and TEAD complexes. In this regard, YAP1-2α(S94A) also formed small puncta independently of TEAD, albeit slightly (Figures 3D and 3F), suggesting potential TEAD-independent mechanisms for weak condensate formation by YAP1-2α.

TAZ forms a homodimer via the Leucine zipper, leading to LLPS independently of YAP1 and TEAD.[39] In contrast, YAP1 cannot form homodimers. TAZ/TAZ-LLPS condensates were similarly produced in both parental and *YAP1*-KO cells (Figure S3I). PLA was used to visualize the interaction between TEAD and HA-tagged YAP1-2α or TAZ. This technique allowed us to distinguish between YAP1-2α/TAZ-LLPS condensates and TAZ/TAZ-LLPS condensates (Figure S3J). Most YAP1-2α/TEAD complexes were localized within YAP1-2α/TAZ-induced LLPS

condensates (Figure S3J, right), whereas TAZ/TEAD complexes were mainly outside TAZ/TAZ-induced LLPS condensates (Figure S3J, left). This indicates the indispensable role of TEAD in YAP1-2α/TAZ/TEAD-LLPS, while TAZ/TAZ-induced puncta likely contain other transcription factors. TAZ/TAZ homodimers were present in TAZ/TAZ-induced LLPS but absent in YAP1-2α/TAZ-LLPS (Figure S3K). These findings demonstrate that YAP1-2α/TAZ/TEAD-LLPS is distinct from TAZ/TAZ-LLPS, the former being formed by YAP1-2α, TAZ, and TEAD complex (YAP1-2α/TAZ/TEAD-LLPS), and the latter by TAZ homodimerization independent of YAP1 and TEAD (TAZ/TAZ-LLPS).

Mechanism of LLPS induction by YAP1/TAZ/TEAD complex formation

YAP1-1 mRNA expression is significantly lower than *YAP1-2* mRNA in various cell types, especially cancer cells.[45] In MDA-MB-436 cells, *YAP1-1α* mRNA expression is about ten times lower than *YAP1-2α* mRNA (Figure S1G). The YAP1-1α isoform possesses a single WW domain and a functional Leucine zipper in its coiled-coil region, allowing it to heterodimerize with TAZ via the Leucine zipper (Figure S4A). To investigate if YAP1-1α induces LLPS, we expressed YAP1-1α or YAP1-2α in MDA-MB-436 cells. YAP1-1α produced fewer nuclear puncta than YAP1-2α, indicating it is significantly less effective in promoting LLPS induction (Figures 4A and S4B).

The WW domain is a protein motif that preferentially interacts with

proline-containing sequences such as PPxY and LPxY motifs.[43,46] LLPS enables the formation of membrane-less puncta or droplets, where specific proteins are concentrated through multivalent interactions.[47] Nuclear puncta/condensates formed via LLPS, including transcription factors, co-activators, and mediators like BRD4 and MED1, are linked to super-enhancer formation. Thus, the presence of BRD4 in nuclear LLPS condensates indicates super-enhances.[48] Mediators are crucial in various transcription aspects, including linking transcription factors to RNA polymerase II (Pol II).[49] The role of BRD4 in LLPS relies on two bromodomains binding to H3K27ac, a marker of active enhancers.[50] Using PLA, we visualized BRD4 and H3K27ac interactions, identifying the BRD4/H3K27ac complex within YAP1-2α/TAZ/TEAD-induced LLPS condensates (Figure S4C). These findings suggest that YAP1-2α/TAZ/TEAD-induced LLPS causes the activation of a super-enhancer. Since BRD4 contains an LPxY motif (LPDY) in bromodomain I and a PPxY motif (PPTY) in its C-terminal proline-rich region (Figure 4B), we hypothesized these motifs interact with the two WW domains of YAP1-2α to facilitate multivalent protein interactions. Protein-protein interaction modeling using AlphaFold2 predicted that YAP1-2α's WW domains (WW1 and WW2) interact with BRD4's PPxY and LPxY motifs (Figures 4C and S4D). Co-immunoprecipitation confirmed YAP1-2α and BRD4 interaction. This interaction was weakened when either PPxY or LPxY motif in BRD4 was disrupted and abolished when both were disrupted (Figure 4D). Similar results were observed using PLA (Figure S4E). The significance

of BRD4 in YAP1-2α/TAZ/TEAD-LLPS condensates was verified by the results that shRNA-mediated BRD4 knockdown and inhibition of YAP1-BRD4 interaction abolished puncta formation (Figures 4E, S4F, and S4G). The reduction in YAP1-2α/TAZ/TEAD-LLPS puncta due to BRD4 knockdown was rescued by ectopic expression of shRNA-resistant wild-type BRD4, but not by BRD4 lacking one or both PPxY/LPxY motifs (Figures 4F and S4H). These findings indicate that BRD4's WW domains are crucial for generating YAP1-2α/TAZ/TEAD-induced LLPS condensates.

Activation of the YAP1-2α/TAZ/TEAD super-enhancer correlates with stem-like malignant properties in cancer cells

To evaluate the impact of YAP1-2α/TAZ/TEAD super-enhancer activation on gene expression, we stably expressed YAP1-2α or YAP1-2γ in MDA-MB-436 cells utilizing a lentiviral infection system. RNA-seq analysis revealed that elevated YAP1-2α expression resulted in the upregulation of 2,006 genes. In contrast, elevated YAP1-2γ expression, which does not induce super-enhancers, led to the upregulation of 3,690 genes compared to controls (Figure S5A). Hallmark gene set analysis revealed distinct signatures for genes upregulated by YAP1-2α and YAP1-2γ (Figure S5B). Subsequently, we investigated the contribution of the YAP1-2α/TAZ/TEAD super-enhancer to the transcriptomic alterations induced by shRNA-mediated knockdown of BRD4, which is essential for super-

enhancer activation.[48,50,51] BRD4 knockdown reduced the expression of 932 out of the YAP1-2α-induced 2,006 genes (Figure 5A and 5B), indicating that these genes are positively regulated by the YAP1-2α/TAZ/TEAD super-enhancer. We subsequently analyzed genes upregulated in PARPi-resistant (Figure 1A) or YAP1-2α-expressing MDA-MB-436 cells and identified 965 genes (Figure 5C), of which 450 genes were dependent on the YAP1-2α/TAZ/TEAD super-enhancer (Figure 5C, left). Hallmark gene set analysis indicated that the 450 genes were strongly associated with EMT (Figures 5C right, S5C and S5D), which plays a crucial role in acquiring cancer stem-like properties.[11-15] The YAP1-2α/TAZ/TEAD super-enhancer may enhance the resilience of cancer cells by potentiating cancer stem-like malignant properties via EMT. Correspondingly, splice variant analysis of PARPi-resistant cancer cells revealed increased expression of CD44 variant isoforms (CD44v), including CD44v9 (Figure 1D and S5E), which are indicators of epithelial cancer stem-like populations.[52,53] These findings support the correlation between elevated YAP1-2α levels and cancer stem-like characteristics. Cell populations exhibiting high levels of CD44v expression were isolated from MDA-MB-436 and UWB1.289 cells utilizing magnetic beads conjugated with an anti-CD44v9 antibody. Although the proportion of CD44v^{high} cells was low, they were present in both MDA-MB-436 and UWB1.289 cells (Figure 5D). The CD44v^{high} cells demonstrated elevated levels of CD44v and YAP1-2α isoforms at both mRNA and protein levels

(Figures 5E and 5F). These CD44v^{high} cells also exhibited activation of genes regulated by the YAP1-2α/TAZ/TEAD super-enhancer, as evidenced by *POLQ* encoding DNA polymerase theta (POLQ), which confers resistance to PARPi in *BRCA*-deficient cancer cells through activation of the microhomology-mediated end-joining (MMEJ) repair pathway[54,55] and *ALDH1A*, a marker of cancer stem-like cells (Figures 5B and 5G).[56] The elevated expression of these genes was inhibited by treatment with JQ1 (Figure 5G), the selective inhibitor of BRD4-regulated super-enhancers.[57] CD44v^{high} cells also exhibited YAP1-2α puncta formation, which were eliminated by JQ1, indicating the activation of the YAP1-2α/TAZ/TEAD super-enhancer in the cells (Figure S5F). These findings suggest that activation of the YAP1-2α/TAZ/TEAD super-enhancer restructures the transcriptional network to promote the acquisition of cancer stem-like properties, thereby increasing the robustness and resilience of cancer cells against various adverse conditions.

Mechanisms by which induction of the YAP1-2α/TAZ/TEAD super-enhancer endows resistance to genotoxic agents

The YAP1-2α/TAZ/TEAD super-enhancer significantly upregulated POLQ, a druggable target in PARPi-resistant *BRCA*-deficient cancers (Figure 5B).[55] To investigate whether the POLQ-MMEJ pathway contributes to resistance to PARPi and Cisplatin, we evaluated the sensitivity of YAP1-2α-overexpressing, PARPi-resistant, or CD44v^{high} *BRCA*-deficient cancer

cells to Olaparib or Cisplatin. The suppression of POLQ expression in these cells significantly reduced MMEJ activity to the level of parental cells (Figures 6A-6C and S6A-S6C). In contrast, POLQ inhibition only partially restored sensitivity to Olaparib or Cisplatin (Figures 6D-6F and S6D). YAP1-2α(LZM), which does not activate the YAP1-2α/TAZ/TEAD super-enhancer, did not induce PARPi resistance (Figure S6E). Therefore, pathways or mechanisms other than the POLQ-MMEJ axis may also exist through which the YAP1-2α/TAZ/TEAD super-enhancer confers PARPi/Cisplatin resistance. Indeed, the super-enhancer regulates genes associated with the acquisition of cancer stem-like properties that enhance drug resistance.[10-15,56] Three-dimensional (3D) cell culture is generally considered superior to two-dimensional (2D) culture for analyzing cancer stem-like properties, as it provides a more physiologically relevant microenvironment that more accurately replicates the *in vivo* conditions of tumors.[58,59] 3D cultures frequently exhibit different drug sensitivities compared to 2D cultures, which may more accurately predict *in vivo* responses.[60,61] Consequently, we re-examined the role of the POLQ-MMEJ axis in PARPi resistance utilizing 3D-cultured spheroids prepared from CD44v^{high} *BRCA*-deficient cancer cells. As observed in 2D cultures, spheroids derived from CD44v^{high} cells demonstrated increased resistance to PARPi and Cisplatin compared to spheroids derived from parental or CD44v^{low} cells (Figure S6F). However, the inhibition of POLQ in CD44v^{high} spheroids only partially restored drug sensitivity (Figure S6G), suggesting again that the induction of POLQ by the YAP1-2α/TAZ/TEAD

super-enhancer does not fully account for the acquisition of resistance to PARPi/Cisplatin in *BRCA*-deficient cancer cells. In contrast, inhibition of the super-enhancer almost fully restored the cell sensitivity to PARPi/Cisplatin (Figures 6G and S6H). Furthermore, sphere-forming activity was enhanced in CD44v^{high} spheroids, which was abolished by inhibiting the formation of the YAP1-2α/TAZ/TEAD super-enhancer (Figures 6H-6K and S6H-S6J), confirming that YAP1-2α/TAZ/TEAD super-enhancer activation conferred cancer stem-like properties. These findings indicated that the acquisition of resistance in *BRCA*-deficient cancer cells to Olaparib and Cisplatin results from the combined effects of cancer stem-like resilience and POLQ, both of which are induced by activation of the YAP1-2α/TAZ/TEAD super-enhancer.

Resistance to anti-cancer drugs correlates with elevated malignant grades of cancer cells

The aforementioned results indicated that the increased drug resistance encompasses enhanced cancer stem-like properties characterized by augmented robustness of malignant phenotypes.[62] Accordingly, we investigated the cancer stem-like properties in YAP1-2α-overexpressing or PARPi-resistant UWB1.289 cells. In 3D culture, these cells demonstrated significantly enhanced sphere-forming activity compared to their parental cells, which was abolished by K-975 or JQ1 treatment (Figures 7A and S7A). YAP1-2α-expressing cells and PARPi-resistant cells also exhibited aggressive characteristics, including enhanced

anchorage-independent growth, higher ferroptosis resistance, increased motility, and elevated invasiveness into the extracellular matrix (Figures 7B, 7C, 7D, 7E, S7B and S7C). They also resisted various anticancer agents, including molecular targeted drugs (Figure S7D). These characteristics are attributable to the activated YAP1-2α/TAZ/TEAD super-enhancer, suggesting that its activation in cancer cells under challenging conditions confers a more aggressive and malignant phenotype compared to their parental cells.

We also analyzed clinical cancer specimens to investigate the enhanced malignant properties of cancer cells. Ovarian cancer tissues exhibiting elevated YAP1-2α expression were associated with increased POLQ expression and more advanced clinical grades (Figures 7F-7I and S7E-S7G). Moreover, in accordance with the *in vitro* findings, tumor regions exhibiting elevated levels of *YAP1-2α* and POLQ expression demonstrated correspondingly higher CD44v expression (Figure 7G, bottom). Analysis of the TCGA dataset further revealed that patients exhibiting higher expression levels of *YAP1* mRNA excluding exon 6 and higher expression levels of *CD44v* mRNA demonstrated significantly poorer prognoses compared to those with lower expression levels of *YAP1* mRNA including exon 6 and lower expression levels of *CD44v* mRNA (Figures 7J and S7H) in both ovarian (OV) and triple-negative breast cancer (TNBC). Consequently, ovarian cancers and TNBCs classified as $CD44v^{high}/YAP1\text{-}2\alpha^{high}$ are associated with poor clinical outcomes, attributable, at least in part, to the activation of the YAP1-2α/TAZ/TEAD

super-enhancer, which increases malignant grades of cancer cells.

To assess the *in vivo* relevance of YAP1-2α/TAZ/TEAD super-enhancer formation, a tumor xenograft assay was conducted utilizing MKN45 human gastric epithelial cells. Subcutaneous inoculation of MKN45 cells ectopically overexpressing YAP1-2α resulted in significantly larger tumors than parental MKN45 cells in nude mice. In contrast, MKN45 cells ectopically expressing mutant YAP1-2α(LZM), which cannot interact with TAZ, exhibited tumor formation comparable to that of parental cells (Figures 7K and S7I). These findings indicated that YAP1-2α/TAZ/TEAD super-enhancer activation enhances the in vivo tumorigenicity of cancer cells.

DISCUSSION

This study demonstrated that prolonged exposure of *BRCA*-deficient cancer cells to genotoxic agents, such as PARPi and Cisplatin, induces the activation of a super-enhancer that potentiates cancer stem-like characteristics with increased malignancy that contributes to therapeutic resistance. The formation of this super-enhancer is initiated by the upregulation of YAP1-2α, a minor isoform of YAP1 that distinctively possesses a Leucine zipper dimerization motif, upon prolonged exposure to PARPi/Cisplatin. Elevated YAP1-2α levels are inversely correlated with reduced levels of major YAP1 isoforms, YAP1-2γ and YAP1-2δ, indicating a shift in the *YAP1* pre-mRNA splicing pattern during the acquisition of drug resistance. Upregulated YAP1-2α heterodimerizes with TAZ via the Leucine zipper without affecting YAP1-2α/TEAD and TAZ/TEAD complex formation. The association of YAP1-2α/TEAD and TAZ/TEAD through the YAP1-2α/TAZ interaction induces LLPS-mediated nuclear condensates, which activate the YAP1-2α/TAZ/TEAD super-enhancer via multivalent interactions between YAP1-2α, TAZ, and BRD4. YAP1-1α can also heterodimerize with TAZ through the Leucine zipper. However, YAP1-1α infrequently induces puncta formation, presumably due to its single WW domain limiting multivalent protein interactions necessary for LLPS (YAP1-2α possesses two WW domains). Independent of YAP1 and TEAD, TAZ promotes LLPS-mediated puncta formation through Leucine zipper-mediated homodimerization. In contrast to TAZ, YAP1-1α and YAP1-2α

cannot homodimerize or heterodimerize owing to the structural incompatibilities between the identical Leucine zipper sequences.[39,40] TAZ is, therefore, associated with a minimum of two distinct super-enhancers: one involving the YAP1-2α/TAZ heterodimer and the other involving the TAZ homodimer, each regulating different sets of target genes.

YAP1 and TAZ regulate numerous genes, including those involved in cell proliferation, cell-cell contact, cell polarity, cellular stress, cell metabolism, and cell cycle.[26-32] Despite their redundant roles in gene regulation, as their primary partner transcription factors are TEADs (TEAD1-4), most studies have suggested that the YAP1/TEAD and TAZ/TEAD transcriptional complexes function independently.[63,64] Eight YAP1 isoforms are generated in human cells by differential splicing of *YAP1* pre-mRNA.[40,42,45,65] Among these, YAP1-2γ and YAP1-2δ, which lack a functional Leucine zipper, are predominantly expressed in both normal and cancer cells. Consequently, our understanding of the YAP1/TAZ heterodimer remained limited until the discovery that YAP1-1α and YAP1-2α are the sole YAP1 isoforms capable of binding TAZ through Leucine zippers.[40] The present study further revealed that YAP1-2α/TAZ heterodimerization activates a super-enhancer comprising YAP1-2α, TAZ, TEAD, and BRD4, which significantly contributed to the acquisition of PARPi/Cisplatin resistance in *BRCA*-deficient cancer cells. Activation of DNA polymerase theta (POLQ), a unique DNA polymerase that is essential for microhomology-mediated end-joining (MMEJ),[54,55] promotes error-prone repair of double-strand breaks (DSBs) induced by

DNA-damaging agents in *BRCA*-deficient cells. This error-prone process also increases the probability of reverse- or second-site mutations in mutated driver genes.[66] However, the induction of POLQ by the super-enhancer cannot fully explain the acquisition of *BRCA*-deficient cell resistance to PARPi/Cisplatin, as the inhibition of POLQ expression only partially restored drug sensitivity, whereas disruption of the YAP1-2α/TAZ/TEAD super-enhancer almost completely abolished drug resistance.

What mechanism underlies the activation of the YAP1-2α/TAZ/TEAD enhancer in conferring substantial resistance to *BRCA*-deficient cells beyond the induction of POLQ? A potential explanation arises from the observation that PARPi/Cisplatin-resistant BRCA-deficient cancer cells with the active YAP1-2α/TAZ/TEAD enhancer also exhibit elevated levels of CD44 variants (CD44v), which are indicators of cancer stem-like cells.[67] The super-enhancer may reconfigure transcriptional networks to potentiate cancer stem-like properties, such as increased self-renewal capacity (3D spheroid formation), enhanced motility and invasion, and elevated resistance to pro-apoptotic signaling. This phenomenon strengthens the malignant characteristics of cancer cells and enhances their resilience to various adverse stresses and conditions. We believe that the activation of the YAP1-2α/TAZ/TEAD super-enhancer may not be specific to *BRCA*-deficient cancer cells exposed to genotoxic stress. Instead, cancer cells subjected to adverse conditions may selectively expand CD44v^{high}/YAP1-2α^{high} cancer stem-like cells, which typically

exist at low frequencies within the cancer cell population, or actively modulate the splicing mechanism of *YAP1* pre-mRNA from a "*YAP1-2γ/δ*-dominant" to a "*YAP1-2α*-dominant" pattern to cope with challenging conditions in a general manner. Consistent with this notion, *BRCA*-deficient cancer cells exhibiting the activated YAP1-2α/TAZ/TEAD super-enhancer also demonstrated increased resistance to the MEK inhibitor Trametinib and the multi-kinase inhibitor Sorafenib, suggesting that the acquisition of resistance to anticancer drugs (including molecular targeted drugs) in *BRCA*-deficient cancers is not limited to DNA-damaging agents.

The YAP1-2α/TAZ/TEAD super-enhancer activates cytokines and chemokines, thereby promoting the polarization and recruitment of myeloid-derived suppressor cells (MDSCs) and tumor-associated macrophages (TAMs), which subsequently inactivate T cells.[68-72] Interferon-γ-induced YAP1 phase separation activates PD-L1,[73] potentially triggering the YAP1-2α/TAZ/TEAD super-enhancer and facilitating immune evasion by cancer cells. YAP1-directed super-enhancers augment cell-intrinsic robustness and facilitate cell-extrinsic conditions that foster cancer cells, establishing a "cold" immune environment and thereby contributing to the malignant progression of cancer.

The present study elucidated an unanticipated molecular connection between alternative mRNA splicing, liquid-liquid phase separation (LLPS), and super-enhancers, which significantly alters cancer cell characteristics without genetic mutations. Recent studies have demonstrated a robust

correlation between aberrant alternative splicing and cancer.[74] The findings of the present study provide valuable insights into the mechanisms by which splicing abnormalities contribute to the progression of cancer. Activating the YAP1-2α/TAZ/TEAD super-enhancer in cancer cells under adverse stresses/conditions confers a more aggressive and malignant phenotype than their parental cells, enabling them to overcome challenging environments. Selective inhibition of differential splicing that generates *YAP1-2α* mRNA impedes cancer progression and mitigates resistance to anticancer therapies.

RESOURCE AVAILABILITY

Lead contact

Further information and requests should be addressed to the lead contact, Masanori Hatakeyama (mhata@m.u-tokyo.ac.jp).

Materials availability

The materials generated in this study are available upon request to the lead contact.

Data and code availability

- All sequencing data created in this study have been uploaded to the Gene Expression Omnibus (GEO; https://www.ncbi.nlm.nih.gov/geo/) and are available under accession code (GSE287274).
- Any additional information required to re-analyze results reported in this manuscript is available upon request to the lead contact.

ACKNOWLEDGMENTS

This work was supported by a JSPS Grant-in-Aid for Scientific Research from the Japan Society for the Promotion of Science Grant numbers 21H04804 (M.H.) 24H00618 (M.H), and JP21K15526 (T.O.), P-PROMOTE from AMED Grant Number JP23ama221219h0001 (M.H.), and Microbial Chemistry Research and Development Fund Grant Number 23A02 (T.O.).

AUTHOR CONTRIBUTIONS

T.O., T.H. (for Prediction of Molecular Complex Structure) and Y. Y. (for qPCR analysis) performed the experiments. T.O. and T.H. analyzed data. T.O. designed the study. T.O. and M.H. wrote the paper. T.H. reviewed the paper. M.H. supervised this work.

DECLARATION OF INTERESTS

The authors declare no competing interests.

STAR★METHODS

All the methods can be found in the online version of this paper and include the following:

- **KEY RESOURCE TABLE**
- **EXPERIMENTAL MODEL AND SUBJECT DETAILS**
  - Cell Lines
  - Three-Dimensional Overlay Culture
  - Mice
  - Human Cancer Patients Data
- **METHOD DETAILS**
  - Expression Vectors
  - Preparation of Lentivirus and Infections
  - RNAi by siRNA or shRNA
  - Detection for Splicing Isoforms
  - Live Cell Imaging
  - Fluorescence Recovery After Photobleaching (FRAP)
  - Immunofluorescence staining
  - Proximity Ligation Assay (PLA)
  - Immunohistochemistry
  - In Situ Hybridization (BaseScope)
  - Immunoprecipitation and Immunoblotting
  - RNA sequencing and Splicing Variant Analysis
  - Quantitative PCR (qPCR)
  - Luciferase Reporter Assay
  - MMEJ Reporter Assay
  - Cell Viability Assay
  - Three-dimensional Cell Viability Assay

- Ferroptosis Assay
- Migration and Invasion Assay
- Prediction of Molecular Complex Structure
- Expression Correlation Analysis
- Kaplan-Meier Analysis
- Tumor Xenograft Assay
- **QUANTIFICATION AND STATISTICAL ANALYSIS**

SUPPLEMENTAL INFORMATION

Supplemental Information includes 7 figures, can be found with this article online.

REFERENCES

1. Min, H.Y., and Lee, H.Y. (2022). Molecular targeted therapy for anticancer treatment. (2022). Exp. Mol. Med. *54*, 1670-1694. https://doi.org/10.1038/s12276-022-00864-3.
2. Goldman, J.M., and Melo, J.V. Targeting the BCR-ABL tyrosine kinase in chronic myeloid leukemia. (2001). N. Engl. J. Med. *344*, 1084-1086. https://doi.org/10.1056/NEJM200104053441409.
3. Cohen, P., Cross, D., and Jänne, P.A. (2021). Kinase drug discovery 20 years after imatinib: progress and future directions. Nat. Rev. Drug Discov. *20*, 551-569. https://doi.org/10.1038/s41573-021-00195-4.
4. Tsao, L.C., Force, J., and Hartman, Z.C. (2021). Mechanisms of therapeutic antitumor monoclonal antibodies. Cancer Res. *81*, 4641-4651. https://doi.org/10.1158/0008-5472.CAN-21-1109.
5. Bhamidipati, D., Haro-Silerio, J.I., Yap, T.A., and Ngoi, N. (2023). PARP inhibitors: enhancing efficacy through rational combinations. Br. J. Cancer *129*, 904-916. https://doi.org/10.1038/s41416-023-02326-7.
6. Lovly, C.M., and Shaw, A.T. (2014). Molecular pathways: resistance to kinase inhibitors and implications for therapeutic strategies. Clin. Cancer Res. *20*, 2249-2256. https://doi.org/10.1158/1078-0432.CCR-13-1610.
7. Panda, M., and Biswal, B.K. (2019). Cell signaling and cancer: a mechanistic insight into drug resistance. Mol. Biol. Rep. *46*, 5645-5659. https://doi.org/10.1007/s11033-019-04958-6.
8. Yuan, S., Norgard, R.J., and Stanger, B.Z. (2019). Cellular plasticity in cancer. Cancer Discov. *9*, 837-851. https://doi.org/10.1158/2159-8290.CD-19-0015.
9. Mani, S.A., Guo, W., Liao, M.J., Eaton, E.N., Ayyanan, A., Zhou, A.Y., Brooks, M., Reinhard, F., Cheng, C.Z., Shipitsin, M., et al. (2008). The epithelial-mesenchymal transition generates cells with properties of stem cells. Cell *133*, 704-715. https://doi.org/10.1016/j.cell.2008.03.027.
10. Hanahan, D. (2022). Hallmarks of cancer: new dimensions. Cancer Discov. *12*, 31-46. https://doi.org/10.1158/2159-8290.CD-21-1059.
11. Pérez González, A.P., Bévant, K., and Blanpain, C. (2023). Cancer cell plasticity during tumor progression, metastasis and response to therapy. Nat. Cancer *8*, 1063-1082. https://doi.org/10.1038/s43018-023-00595-y.

12. Loh, J.J., and Ma, S. (2024). Hallmarks of cancer stemness. Cell Stem Cell *31*, 617-639. https://doi.org/10.1016/j.astem.2024.04.004.

13. Bocci, F., Gearhart-Serna, L., Boareto, M., Ribeiro, M., Ben-Jacob, E., Devi, G.R., Levine, H., Onuchic, J.N., and Jolly, M.K. (2019). Toward understanding cancer stem cell heterogeneity in the tumor microenvironment. Proc. Natl. Acad. Sci. USA. *116*, 148-157. https://doi.org/10.1073/pnas.1815345116.

14. Gupta, P.B., Chaffer, C.L., and Weinberg, R.A. (2009). Cancer stem cells: mirage or reality? Nat. Med. *15*, 1010-1012. https://doi.org/10.1038/nm0909-1010.

15. Singh, A., and Settleman, J. (2010). EMT, cancer stem cells and drug resistance: an emerging axis of evil in the war on cancer. Oncogene *29*, 4741-4751. https://doi.org/10.1038/onc.2010.215.

16. Sengupta, S. and George, R.E. (2017). Super-enhancer-driven transcriptional dependencies in cancer. Trends Cancer *3*, 269-281. https://doi.org/10.1016/j.trecan.2017.03.006.

17. Sabari, B.R., Dall'Agnese, A., Boija, A., Klein, I.A., Coffey, E.L., Shrinivas, K., Abraham, B.J., Hannett, N.M., Zamudio, A.V., Manteiga, J.C., et al. (2018). Coactivator condensation at super-enhancers links phase separation and gene control. Science *361*, eaar3958. https://doi.org/10.1126/science.

18. Laflamme, G., and Mekhail, K. (2020). Biomolecular condensates as arbiters of biochemical reactions inside the nucleus. Commun. Biol. *3*, 773. https://doi.org/10.1038/s42003-020-01517-9.

19. Tan, M., Pan, Q., Gong, H., Zhai, X., Wan, Z., Ge, M., Gu, J., Zhang, D., Chen, X., and Xu, D. (2023). Super-enhancer-associated SNHG15 cooperating with FOSL1 contributes to bladder cancer progression through the WNT pathway. Pharmacol. Res. *197*, 106940. https://doi.org/10.1016/j.phrs.2023.106940.

20. Luo, S., Luo, Y., Wang, Z., Yin, H., Wu, Q., Du, X., and Xie, X. (2024). Super-enhancer mediated upregulation of MYEOV suppresses ferroptosis in lung adenocarcinoma. Cancer Lett. *589*, 216811. https://doi.org/10.1016/j.canlet.2024.216811.

21. Hu, X., Wu, J., Feng, Y., Ma, H., Zhang, E., Zhang, C., Sun, Q., Wang, T., Ge, Y., Zong, D., et al. (2023). METTL3-stabilized super enhancers-lncRNA SUCLG2-AS1 mediates the formation of a long-range chromatin loop between enhancers and promoters of SOX2

in metastasis and radiosensitivity of nasopharyngeal carcinoma. Clin. Transl. Med. *13*, e1361. https://doi.org/10.1002/ctm2.1361.

22. Hazan, I., Monin, J., Bouwman, B.A.M., Crosetto, N., and Aqeilan, R.I. (2019). Activation of oncogenic super-enhancers is coupled with DNA repair by RAD51. Cell Rep. *15*, 560-572. https://doi.org/10.1016/j.celrep.2019.09.001.

23. Tasdemir, N., Banito, A., Roe, J.S., Alonso-Curbelo, D., Camiolo, M., Tschaharganeh, D.F., Huang, C.H., Aksoy, O., Bolden, J.E., Chen, C.C., et al. (2016). BRD4 connects enhancer remodeling to senescence immune surveillance. Cancer Discov. *6*, 612-629. https://doi.org/10.1158/2159-8290.CD-16-0217.

24. Ruscetti, M., Morris, J.P. 4th., Mezzadra, R., Russell, J., Leibold, J., Romesser, P.B., Simon, J., Kulick, A., Ho, Y.J., Fennell, M., et al. (2020). Senescence-induced vascular remodeling creates therapeutic vulnerabilities in pancreas cancer. Cell *181*, 424-441. https://doi.org/10.1016/j.cell.2020.03.008.

25. Li, G.H., Qu, Q., Qi, T.T., Teng, X.Q., Zhu, H.H., Wang, J.J., Lu, Q., and Qu, J. (2021). Super-enhancers: a new frontier for epigenetic modifiers in cancer chemoresistance. J. Exp. Clin. Cancer Res. *40*, 174. https://doi.org/10.1186/s13046-021-01974-y.

26. Zanconato, F., Cordenonsi, M., and Piccolo, S. (2016). YAP/TAZ at the roots of cancer. Cancer Cell *29*, 783-803. https://doi.org/10.1016/j.ccell.2016.05.005.

27. Zhao, B., Ye, X., Yu, J., Li, L., Li, W., Li, S., Yu, J., Lin, J.D., Wang, C.Y., Chinnaiyan, A.M., et al. (2008). TEAD mediates YAP-dependent gene induction and growth control. Genes Dev. *22*, 1962-1971. https://doi.org/10.1101/gad.1664408.

28. Zhang, H., Liu, C.Y., Zha, Z.Y., Zhao, B., Yao, J., Zhao, S., Xiong, Y., Lei, Q.Y., and Guan, K.L. (2009). TEAD transcription factors mediate the function of TAZ in cell growth and epithelial-mesenchymal transition. J. Biol. Chem. *284*, 13355-13362. https://doi.org/10.1074/jbc.M900843200.

29. Zheng, Y., and Pan, D. (2019). The Hippo signaling pathway in development and disease. Dev. Cell *50*, 264-282. https://doi.org/10.1016/j.devcel.2019.06.003.

30. Heng, B.C., Zhang, X., Aubel, D., Bai,Y., Li, X., Wei, Y., Fussenegger, M., and Deng, X. (2021). An overview of signaling pathways regulating YAP/TAZ activity. Cell. Mol. Life Sci. *78*, 497-512. https://doi.org/10.1007/s00018-020-03579-8.

31. Fu, V., Plouffe, S.W., and Guan, K.L. (2017). The Hippo pathway in organ development, homeostasis, and regeneration. Curr. Opin. Cell Biol. *49*, 99-107. https://doi.org/10.1016/j.ceb.2017.12.012.

32. Kim, M.H., and Kim, J. (2017). Role of YAP/TAZ transcriptional regulators in resistance to anti-cancer therapies. Cell. Mol. Life Sci. *74*, 1457-1474. https://doi.org/10.1007/s00018-016-2412-x.

33. Shao, D.D., Xue, W., Krall, E.B., Bhutkar, A., Piccioni, F., Wang, X., Schinzel, A.C., Sood, S., Rosenbluh, J., Kim, J.W., et al. (2014). KRAS and YAP1 converge to regulate EMT and tumor survival. Cell *158*, 171-184. https://doi.org/10.1016/j.cell.2014.06.004.

34. Pham, T.H., Hagenbeek, T.J., Lee, H.J., Li, J., Rose, C.M., Lin, E., Yu, M., Martin, S.E., Piskol, R., Lacap, J.A., et al. (2021). Machine-learning and chemicogenomics approach defines and predicts cross-talk of Hippo and MAPK pathways. Cancer Discov. *11*, 778-793. https://doi.org/10.1158/2159-8290.CD-20-0706.

35. Lin, L., Sabnis, A.J., Chan, E., Olivas, V., Cade, L., Pazarentzos, E., Asthana, S., Neel, D., Yan, J.J., Lu, X., et al. (2015). The Hippo effector YAP promotes resistance to RAF- and MEK-targeted cancer therapies. Nat. Genet. *47*, 250-256. https://doi.org/10.1038/ng.3218.

36. Thrash, H.L., and Pendergast, A.M. (2023). Multi-functional regulation by YAP/TAZ signaling networks in tumor progression and metastasis. Cancers *15*, 4701. https://doi.org/10.3390/cancers15194701.

37. Zanconato, F., Forcato, M., Battilana, G., Azzolin, L., Quaranta, E., Bodega, B., Rosato, A., Bicciato, S., Cordenonsi, M., and Piccolo, S. (2015). Genome-wide association between YAP/TAZ/TEAD and AP-1 at enhancers drives oncogenic growth. Nat. Cell Biol. *17*, 1218-1227. https://doi.org/10.1038/ncb3216.

38. He, L., Pratt, H., Gao, M., Wei, F., Weng, Z., and Struhl, K. (2021). YAP and TAZ are transcriptional co-activators of AP-1 proteins and STAT3 during breast cellular transformation. Elife *10*, e67312. https://doi.org/10.7554/eLife.67312.

39. Lu, Y., Wu, T., Gutman, O., Lu, H., Zhou, Q., Henis, Y.I., and Luo, X. (2020). Phase separation of TAZ compartmentalizes the transcription machinery to promote gene expression. Nat. Cell Biol. *22*, 453-464. https://doi.org/10.1038/s41556-020-0485-0.

40. Ben, C., Takahashi-Kanemitsu, A., Wu, X., Knight, C.K., and Hatakeyama, M. (2020). Alternative splicing reverses the cell-intrinsic and cell-extrinsic prooncogenic potentials

of YAP1 via SHP2. J. Biol. Chem. *295*, 13965-13980. https://doi.org/10.1074/jbc.RA120.013820.

41. Kim, C., Wang, X.D., and Yu, Y. (2020). PARP1 inhibitors trigger innate immunity via PARP1 trapping-induced DNA damage response. Elife *9*, e60637. https://doi.org/10.7554/eLife.60637.

42. Gaffney, C.J., Oka, T., Mazack, V., Hilman, D., Gat, U., Muramatsu, T., Inazawa, J., Golden, A., Carey, D.J., Farooq, A., et al. (2012). Identification, basic characterization and evolutionary analysis of differentially spliced mRNA isoforms of human YAP1 gene. Gene *509*, 215-222. https://doi.10.1016/j.gene.2012.08.025.

43. Ingham, R.J., Colwill, K., Howard, C., Dettwiler, S., Lim, C.S.H., Yu, J., Hersi, K., Raaijmakers, J., Gish, G., Mbamalu, G., et al. (2005). WW domains provide a platform for the assembly of multiprotein networks. Mol. Cell. Biol. *25*, 7092-7106. https://doi: 10.1128/MCB.25.16.7092-7106.2005

44. Kaneda, A., Seike, T., Danjo, T., Nakajima, T., Otsubo, N., Yamaguchi, D., Tsuji, Y., Hamaguchi, K., Yasunaga, M., and Nishiya, Y., et al. (2020). The novel potent TEAD inhibitor, K-975, inhibits YAP1/TAZ-TEAD protein-protein interactions and exerts an anti-tumor effect on malignant pleural mesothelioma. Am. J. Cancer Res. *10*, 4399-4415.

45. Guo, Q., Quan, M., Dong, J., Bai, J., Wang, J., Han, R., Wang, W., Cai, Y., et al. (2020). The WW domains dictate isoform-specific regulation of YAP1 stability and pancreatic cancer cell malignancy. Theranostics *10*, 4422-4436. https://doi.org/10.7150/thno.42795.

46. Hatstat, A.K., Pupi, M.D., and McCafferty, D.G. (2021). Predicting PY motif-mediated protein-protein interactions in the Nedd4 family of ubiquitin ligases. PLoS One *16*, e0258315. https://doi.org/10.1371/journal.pone.0258315.

47. Mehta, S., and Zhang, J. (2022). Liquid-liquid phase separation drives cellular function and dysfunction in cancer. Nat. Rev. Cancer *22*, 239-252. https://doi.org/10.1038/s41568-022-00444-7.

48. Qian, H., Zhu, M., Tan, X., Zhang, Y., Liu, X., and Yang, L. (2023). Super-enhancers and the super-enhancer reader BRD4: tumorigenic factors and therapeutic targets. Cell Death Discov. *9*, 470. https://doi.org/10.1038/s41420-023-01775-6.

49. Conaway, R.C., and Conaway, J.W. (2011). Function and regulation of the mediator complex. Curr. Opin. Genet. Dev. *21*, 225-230. https://doi.org/10.1016/j.gde.2011.01.013.

50. Han, X., Yu, D., Gu, R., Jia, Y., Wang, Q., Jaganathan, A., Yang, X., Yu, M., Babault, N., Zhao, C., et al. (2020). Roles of the BRD4 short isoform in phase separation and active gene transcription. Nat. Struct. Mol. Biol. *27*, 333-341. https://doi.org/10.1038/s41594-020-0394-8.

51. Bacabac, M., and Xu, W. (2023). Oncogenic super-enhancers in cancer: mechanisms and therapeutic targets. Cancer Metastasis Rev. *42*, 471-480. https://doi.org/10.1007/s10555-023-10103-4.

52. Hu, J., Li, G., Zhang, P., Zhuang, X., and Hu, G. (2017). A CD44v^{+} subpopulation of breast cancer stem-like cells with enhanced lung metastasis capacity. Cell Death Dis. *8*, e2679. https://doi.org/10.1038/cddis.2017.72.

53. Nagano, O., Okazaki, S., and Saya, H. (2013). Redox regulation in stem-like cancer cells by CD44 variant isoforms. Oncogene *32*, 5191-5198. https://doi.org/10.1038/onc.2012.638.

54. Ceccaldi, R., Liu, J.C., Amunugama, R., Hajdu, I., Primack, B., Petalcorin, M.I., O'Connor, K.W., Konstantinopoulos, P.A., Elledge, S.J., Boulton, S.J., et al. (2015). Homologous-recombination-deficient tumours are dependent on Polθ-mediated repair. Nature *518*, 258-262. https://doi.org/10.1038/nature14184.

55. Baxter, J.S., Zatreanu, D., Pettitt, S.J., and Lord, C.J. (2022). Resistance to DNA repair inhibitors in cancer. Mol. Oncol. *16*, 3811-3827. https://doi.org/10.1002/1878-0261.13224.

56. Martinez-Cruzado, L., Tornin, J., Santos, L., Rodriguez, A., García-Castro, J., Morís, F., and Rodriguez, R. (2016). Aldh1 expression and activity increase during tumor evolution in sarcoma cancer stem cell populations. Sci. Rep. *6*, 27878. https://doi.org/10.1038/srep27878.

57. Filippakopoulos, P., Qi, J., Picaud, S., Shen, Y., Smith, W.B., Fedorov, O., Morse, E.M., Keates, T., Hickman, T.T., Felletar, I., et al. (2010). Selective inhibition of BET bromodomains. Nature *468*, 1067-1073. https://doi.org/10.1038/nature09504.

58. Zhang, C., Yang, Z., Dong, D.L., Jang, T.S., Knowles, J.C., Kim, H.W., Jin, G.Z., and Xuan, Y. (2020). 3D culture technologies of cancer stem cells: promising ex vivo tumor models. J. Tissue Eng. *11*, 1-17. https://doi.org/10.1177/2041731420933407.

59. Abbas, Z.N., Al-Saffar, A.Z., Jasim, S.M., and Sulaiman, G.M. (2023). Comparative analysis between 2D and 3D colorectal cancer culture models for insights into cellular

morphological and transcriptomic variations. Sci. Rep. *13*, 18380. https://doi.org/10.1038/s41598-023-45144-w.

60. Lv, D., Hu, Z., Lu, L., Lu, H., and Xu, X. (2017). Three-dimensional cell culture: A powerful tool in tumor research and drug discovery. Oncol. Lett. *14*, 6999-7010. https://doi.org/10.3892/ol.2017.7134.
61. Paolillo, M., Colombo, R., Serra, M., Belvisi, L., Papetti, A., Ciusani, E., Comincini, S., and Schinelli, S. (2019). Stem-like cancer cells in a dynamic 3D culture system: A model to study metastatic cell adhesion and anti-cancer drugs. Cells *8*, 1434. https://doi.org/10.3390/cells8111434.
62. Hanahan, D., and Weinberg, R.A. The hallmarks of cancer. (2000). Cell *100*, 57-70. https://doi.org/10.1016/s0092-8674(00)81683-9.
63. Kaan, H.Y.K., Chan, S.W., Tan, S.K.J., Guo, F., Lim, C.J., Hong, W., and Song, H. (2017). Crystal structure of TAZ-TEAD complex reveals a distinct interaction mode from that of YAP-TEAD complex. Sci. Rep. *7*, 2035. https://doi.org/10.1038/s41598-017-02219-9.
64. Cunningham, R., and Hansen, C.G. (2022). The Hippo pathway in cancer: YAP/TAZ and TEAD as therapeutic targets in cancer. Clin. Sci. (Lond) *136*, 197-222. https://doi.org/10.1042/CS20201474.
65. Sudol, M. (2013). YAP1 oncogene and its eight isoforms. Oncogene *32*, 3922. https://doi.org/10.1038/onc.2012.520.
66. Pettitt, S.J., Frankum, J.R., Punta, M., Lise, S., Alexander, J., Chen, Y., Yap, T.A., Haider, S., Tutt, A.N.J. and Lord, C.J. (2020). Clinical *BRCA1/2* reversion analysis identifies hotspot mutations and predicted neoantigens associated with therapy resistance. Cancer Discov. *10*, 1475-1488. https://doi.org/10.1158/2159-8290.CD-19-1485.
67. Yan, Y., Zuo, X., and Wei, D. (2015). Concise review: Emerging role of CD44 in cancer stem cells: A promising biomarker and therapeutic target. Stem Cells Transl. Med. *4*, 1033-1043. https://doi.org/10.5966/sctm.2015-0048.
68. Hao, F. (2022). An overview of the crosstalk between YAP and cGAS-STING signaling in non-small cell lung cancer: it takes two to tango. Clin. Transl. Oncol. *24*, 1661-1672. https://doi.org/10.1007/s12094-022-02826-7.
69. Wang, S., Zhou, L., Ling, L., Meng, X., Chu, F., Zhang, S., and Zhou, F. (2020). The crosstalk between Hippo-YAP pathway and innate immunity. Front. Immunol. *11*, 323. https://doi.org/10.3389/fimmu.2020.00323.

70. Wang, G., Lu, X., Dey, P., Deng, P., Wu, C.C., Jiang, S., Fang, Z., Zhao, K., Konaparthi, R., Hua, S., et al. (2016). Targeting YAP-dependent MDSC infiltration impairs tumor progression. Cancer Discov. *6*, 80-95. https://doi.org/10.1158/2159-8290.CD-15-0224.

71. Yang, W., Yang, S., Zhang, F., Cheng, F., Wang, X., and Rao, J. (2020). Influence of the Hippo-YAP signalling pathway on tumor associated macrophages (TAMs) and its implications on cancer immunosuppressive microenvironment. Ann. Transl. Med. *8*, 399. https://doi.org/10.21037/atm.2020.02.11.

72. Lee, B.S., Park, D.I., Lee, D.H., Lee, J.E., Yeo, M.K., Park, Y.H., Lim, D.S., Choi, W., Lee, D.H., Yoo, G., et al. (2017). Hippo effector YAP directly regulates the expression of PD-L1 transcripts in EGFR-TKI-resistant lung adenocarcinoma. Biochem. Biophys. Res. Commun. *491*, 493-499. https://doi.org/10.1016/j.bbrc.2017.07.007.

73. Yu, M., Peng, Z., Qin, M., Liu, Y., Wang, J., Zhang, C., Lin, J., Dong, T., Wang, L., Li, S., et al. (2021). Interferon-γ induces tumor resistance to anti-PD-1 immunotherapy by promoting YAP phase separation. Mol. Cell *81*, 1216-1230. https://doi.org/10.1016/j.molcel.2021.01.010.

74. Bradley, R.K., and Anczukow, O. (2023). RNA splicing dysregulation and the hallmarks of cancer. Nat. Rev. Cancer *23*, 135-155. https://doi.org/10.1038/s41568-022-00541-7.

75. Ooki, T., Murata-Kamiya, N., Takahashi-Kanemitsu, A., Wu, W. and Hatakeyama, M. (2019). High-Molecular-Weight hyaluronan is a Hippo pathway ligand directing cell density-dependent growth inhibition via PAR1b. (2019). Dev. Cell 49, 590-604. https://doi.org/10.1016/j.devcel.2019.04.018.

76. Cerami, E., Gao, J., Dogrusoz, U., Gross, B.E., Sumer, S.O., Aksoy, B.A., Jacobsen, A., Byrne, C.J., Heuer, M.L., Larsson, E., et al. (2012). The cBio cancer genomics portal: an open platform for exploring multidimensional cancer genomics data. Cancer Discov. *2*, 401-404. https://doi.org/10.1158/2159-8290.

77. Gao, J., Aksoy, B.A., Dogrusoz, U., Dresdner, G., Gross, B., Sumer, S.O., Sun, Y., Jacobsen, A., Sinha, R., Larsson, E., et al. (2013). Integrative analysis of complex cancer genomics and clinical profiles using the cBioPortal. Sci. Signal. *6*, pl1. https://doi.org/10.1126/scisignal.2004088.

78. de Bruijn, I., Kundra, R., Mastrogiacomo, B., Tran, T.N., Sikina, L., Mazor, T., Li, X., Ochoa, A., Zhao, G., Lai, B., et al. (2023). Analysis and visualization of longitudinal genomic and clinical data from the AACR project GENIE Biopharma Collaborative in

cBioPortal. Cancer Res. *83*, 3861-3867. https://doi.org/10.1158/0008-5472.CAN-23-0816.

79. Ryan, M., Wong, W.C., Brown, R., Akbani, R., Su, X., Broom, B., Melott, J., and Weinstein. (2016). J. TCGASpliceSeq a compendium of alternative mRNA splicing in cancer. Nucleic Acids Res. *44*, D1018-1122. https://doi.org/10.1093/nar/gkv1288.

80. Ooki, T., and Hatakeyama, M. (2012). Protocol for visualizing conditional interaction between transmembrane and cytoplasmic proteins. STAR Protoc. *2*, 100430. https://doi.org/10.1016/j.xpro.2021.100430.

81. Zhou, Y., Zhou, B., Pache, L., Chang, M., Khodabakhshi, A.H., Tanaseichuk, O., Benner, C., and Chanda, S.K. (2019). Metascape provides a biologist-oriented resource for the analysis of systems-level datasets. Nat. Commun. *10*, 1523. https://doi.org/10.1038/s41467-019-09234-6.

FIGURE LEGENDS

Figure 1. Cancer cell resistance to genotoxic agents is associated with the upregulation of a minor YAP1 isoform, YAP1-2α

(A) RNA-seq analysis of PARPi-resistant MDA-MB-436 and UWB1.289 cells (n=3 per cell line). See Figures S1A and S1E.

(B) Heat maps showing the changes in the expression of Hippo signaling-related genes. n=3 for each group.

(C) Inclusion/exclusion of exon 6 in *YAP1* mRNA. Two independent PARPi-resistant cells (R1 and R2) for each *BRCA*-deficient cell line were used.

(D and E) Comprehensive alternative splicing analysis. (D) Genes with altered exons and exon-exon junctions in PARPi-resistant cells. (E) Changes in *YAP1* exons and exon-exon junctions (left panel). Bar graphs indicate significantly altered exons (red lines) and exon-exon junctions (pink lines) (right panel). Exons 1 and 3 of *YAP1* were used as negative controls. See Figure S1G.

(F) Three independent Cisplatin-resistant cell lines were established from UBW1.289 cells. MTS assay (top) and PCR analysis for exon 6 detection in *YAP1* mRNAs (bottom).

(G) *BRCA*-deficient cells transduced with the indicated YAP1 isoforms using lentiviruses. Sensitivity of cells to Olaparib or Cisplatin (right). (F and G) Error bars indicate the mean ± SD. n=3.

Figure 2. Elevated YAP1-2α induces LLPS through heterodimerization with TAZ

(A) YAP1-immunofluorescence staining of PARPi-resistant UWB1.289 cells treated with or without Hex. The bottom panels are magnified images of the cells, as indicated by the yellow arrows in the top panels.

(B) Immunoblotting of endogenous YAP1-1, YAP1-2, and mVenus-fused YAP1 isoforms.

(C) The fluorescence signal of mVenus (green). See Figures S2C and S2D.

(D) Percentage of cells with nuclear YAP1 puncta is shown in (C). ***$p < 0.001$; n.s., not significant (ANOVA post-Bonferroni). n=3. Error bars indicate SEM. See Figure S2D.

(E) Reconstitution of *YAP1*-knockout cells with a single YAP1 splicing isoform, YAP1-2α or YAP1-2γ (right panel). YAP1-2α-specific puncta formation was determined by immunofluorescence staining (left panel). (F and G) Live cell imaging of *YAP1*-KO UWB1.289 cells transfected with mVenus-fused YAP1-2α. (F) Yellow arrows indicate punctate fusion. (G) Fluorescence signals at the indicated time points after Hex treatment.

(H and I) FRAP analysis of the mVenus-fused YAP1-2α. (H) Time-lapse images of two independent *YAP1*-KO UWB1.289 cells transfected with mVenus-fused YAP1-2α are shown in Exp.1 and Exp.2. Yellow arrows indicate photobleached puncta. Images of the entire nucleus are shown in Figure S2E. Unbleached puncta were used as negative controls. Scale bars indicate 1 μm. (I) Fluorescence intensities of puncta (photobleached,

n=12; unbleached, n=12) were analyzed from a series of time-lapse images. τ: interval of fluorescence detection. Error bars indicate the mean ± SD. (A, C, E, F, and G) Scale bars indicate 10 μm.

Figure 3. LLPS induced by the YAP1-2α/TAZ heterodimer activates a super-enhancer

(A) Nuclear puncta formation in *YAP1*-KO UWB1.289 cells expressing the mVenus-fused YAP1-2α mutants. See Figure S3B.

(B) Interaction of YAP1-2α with TAZ, as visualized using PLA in UWB1.289 cells. Red dots: PL spots, green: mVenus fluorescence, yellow dots: colocalization of YAP1-2α puncta and PL spots.

(C) Formation of YAP1-2α puncta in the *TAZ*-KO MDA-MB-436 cells (left panel). Number of YAP1-2α puncta in the nucleus (right panel). See Figure S3E.

(D and E) The Interaction of YAP1-2α mutants with TEAD was visualized using PLA. (D) Immunofluorescence images of mVenus-fused YAP1-2α (green) complexed with TEAD (red). The puncta indicated by white arrows are enlarged in the bottom row. See Figure S3G. (E) Co-localization of the YAP1-2α puncta and YAP1-2α/TEAD PL spots. Green circles: number of nuclear YAP1-2α puncta, red circles: number of nuclear PL spots, yellow circles: number of colocalized puncta and spots. n=20 nuclei.

(F) Wild-type YAP1-2α(WT) or YAP1-2α(S94A)-transfected cells were treated with K-975. See Figure S3H. TEAD dependency of LLPS-mediated

YAP1-2α puncta (left panel). Number of YAP1-2α puncta in the nucleus (right panel).

(A, C, and F) ***$p < 0.001$; n.s., not significant (A: Kruskal-Wallis post Bonferroni, C and F: Mann-Whitney U test). n=3. Error bars indicate the median ± SE. All scale bars represent 10 μm.

Figure 4. YAP1-2α/TAZ-induced super-enhancer formation requires TEAD and BRD4

(A) Puncta formation of YAP1-1α and YAP1-2α. Schematic diagrams of YAP1-1α and YAP1-2α (top panel). The fluorescence signal of mVenus (bottom left). Number of YAP1 puncta in the nucleus (bottom right). See Figure S4B.

(B) Schematic diagram of BRD4.

(C) Structural prediction of the interaction between YAP1-2α and BRD4 using AlphaFold2. The WW2 domain (grey), LPxY motif (blue), and PPxY motif (magenta) are shown in the ribbon diagram (top). The vacuum electrostatic surface of the WW2 domain is represented in red (acidic) to blue (basic) (middle). The buried surface area of the LPxY and PPxY motifs in the complex (bottom). See Figure S4D.

(D) Interaction between YAP1-2α and BRD4 in MDA-MB-436 cells.

(E) Effect of BRD4 inhibition on YAP1-2α puncta formation in MDA-MB-436 cells. Cells transfected with shBRD4 were marked by GFP (green). mCherry-fused YAP1-2α (red). The cells indicated by white arrows were

magnified, and the number of YAP1-2α puncta in the nucleus was calculated (top right). BRD4 was knocked down using two different shRNAs (#1 and #2) (bottom right).

(F) Genetic rescue of the shBRD4-mediated reduction in YAP1-2α puncta formation by shBRD4-resistant BRD4. See Figure S4H. YAP1-2α (red), Flag-BRD4 (gray), nuclei (blue). The area indicated by the yellow dashed box is enlarged (bottom left). Yellow arrows indicate the colocalization of YAP1-2α puncta and BRD4. The number of YAP1-2α puncta in the nucleus is shown (right).

(A, E, and F) n=3, ***$p < 0.001$; **$p < 0.01$; *$p < 0.05$; n.s., not significant (Kruskal-Wallis post Bonferroni). Error bars indicate the median ± SE. All scale bars represent 10 μm.

Figure 5. Rewiring of the transcriptional network by the YAP1-2α/TAZ/TEAD super-enhancer confers stem-like malignant properties

(A) Genes downregulated by BRD4 inhibition in MDA-MB-436 cells overexpressing YAP1-2α (left, n=3). BRD4 knockdown was confirmed by immunoblotting (right). See Figures S5A and S5B.

(B) LLPS dependence of the 932 genes upregulated by the YAP1-2α super-enhancer. Blue bars: fold increase (YAP1-2α/Control), black bars: fold decrease (shBRD4/shControl in YAP1-2α-overexpressing cells). See Figures S5C and S5D.

(C) Genes upregulated in both PARPi-resistant and YAP1-2α-overexpressing MDA-MB-436 cells (left). Hallmark gene set analysis (right).

(D) Pie charts showing CD44v9^{high} populations in parental UWB1.289 and MDA-MB-436 cells.

(E) Qualitative splice variant analysis of *CD44* (top) and *YAP1* (bottom) mRNAs by PCR.

(F) *YAP1-2α* mRNA and CD44v9 protein expression were detected using *in situ* RNA hybridization (BaseScope) and immunofluorescence staining, respectively. Scale bars represent 10μm.

(G) qPCR analysis of *POLQ* (upper) and *ALDH1A3* (lower) mRNA expressions. n=3, ***$p < 0.001$; **$p < 0.01$, (ANOVA post-Bonferroni). Error bars indicate the median ± SD.

Figure 6. YAP1-2α/TAZ/TEAD super-enhancer induces cancer stem-like properties with elevated MMEJ activity

(A-F) Cells transfected with siControl or siPOLQ were subjected to the MMEJ reporter assay **(**A to C**)** or MTS assay **(**D to F**).** See Figures S6A-S6C.

(A-C) The Effect of POLQ knockdown on MMEJ activity. (A) YAP1-2α-overexpressing MDA-MB-436 cells. (B) PARPi-resistant MDA-MB-436 cells. (C) CD44v^{high} UWB1.289 cells. Scale bars represent 10 μm.

(D-F) Sensitivity of cells to Olaparib or Cisplatin. (D) YAP1-2α-overexpressing MDA-MB-436 cells. (E) PARPi-resistant MDA-MB-436 cells. (F) CD44v^{high} UWB1.289 cells. See Figure S6D for consideration of the off-target effects of the siRNAs.

(G) Sensitivities of CD44v^{high} UWB1.289 spheroids treated with K-975 or JQ1 to Olaparib or Cisplatin determined by 3D cell viability assay. See Figure S6H.

(H) Growth of CD44v^{high} UWB1.289 spheroids treated with JQ1 or K-975, as measured by 3D cell viability assay (right). Bright-field images (left). Scale bars represent 200 μm. See Figure S6H.

(I-K) 3D culture of CD44v^{high} UWB1.289 cells treated with or without JQ1. (I) Bright-field images of the spheroids. Scale bars represent 200 μm. (J) Three-dimensional reconstructed images of the spheroids. (K) Single-slice images of the spheroids. See Figures S6I and S6J. (J and K) Scale bars represent 10 μm.

(A, B, C, G, and H) ***$p < 0.001$; **$p < 0.01$; *$p < 0.05$. n.s., not significant (ANOVA post-Bonferroni). (A-H) Error bars indicate the mean ± SD. n=3.

Figure 7. The YAP1-2α/TAZ/TEAD super-enhancer strengthens cancer cell robustness and potentiates malignant characteristics

(A-E) YAP1-2α-overexpressing, YAP1-2γ-overexpressing, or PARPi-resistant UWB1.289 cells were treated with K-975 or JQ1. See Figures

S7A-S7C. (A) Bright-field images and ki-67 staining of 3D-cultured spheroids. The Feret diameter of the spheroids is shown in the graph (bottom right). Red bars represent mean values. (B) Anchorage-independent 3D cell growth. (C) Invasion assay. (D) Migration assay. (E) Ferroptosis (left) and lipid hydroperoxide (right) assays. See Figure S7B. (B-E) n=3. Error bars indicate mean ± SD.

(F-I) Sequential tissue sections derived from patients with high-grade serous ovarian cancer. See Figures S7E and S7F. (F) HE staining. (G) CD44v9 (magenta) and POLQ (green) staining. *YAP1-2α* mRNA (red) was visualized using BaseScope. The dashed box area was enlarged (red box: tumor region in which *YAP1-2α*^{low} cells were enriched. Yellow box: the region in which both *YAP1-2α*^{high} and YAP1-2α^{low} tumor cells coexist in a mixture). (H) Correlation between the POLQ protein and *YAP1-2α* mRNA expression using scatter plots (r: Pearson's correlation coefficient). (I) Correlation between clinical stage and expression levels of *YAP1-2α* mRNA (left) or POLQ protein (right). The Boxes include the 25th–75th percentiles, with bars indicating means and whiskers indicating the range of data.

(J) Overall survival rates of patients in TCGA cohort using Kaplan-Meier curves. Ovarian cancer (OV). Triple-negative breast cancer (TNBC). See Figure S7H.

(K) Nude mice were subcutaneously inoculated with MKN45 gastric cancer cells ectopically expressing YAP1-2α(WT) or YAP1-2α(LZM). The

dot plots show the tumor volumes measured 20 d after inoculation (n=12 for each group). Red bars indicate the mean tumor volumes. See Figure S7I.

(A-E, I, J, and K) ***$p < 0.001$; **$p < 0.01$; *$p < 0.05$; n.s., not significant (A-E, I, and K: ANOVA post-Bonferroni, J: log-rank test). All scale bars represent 100 μm.

Figure 1.

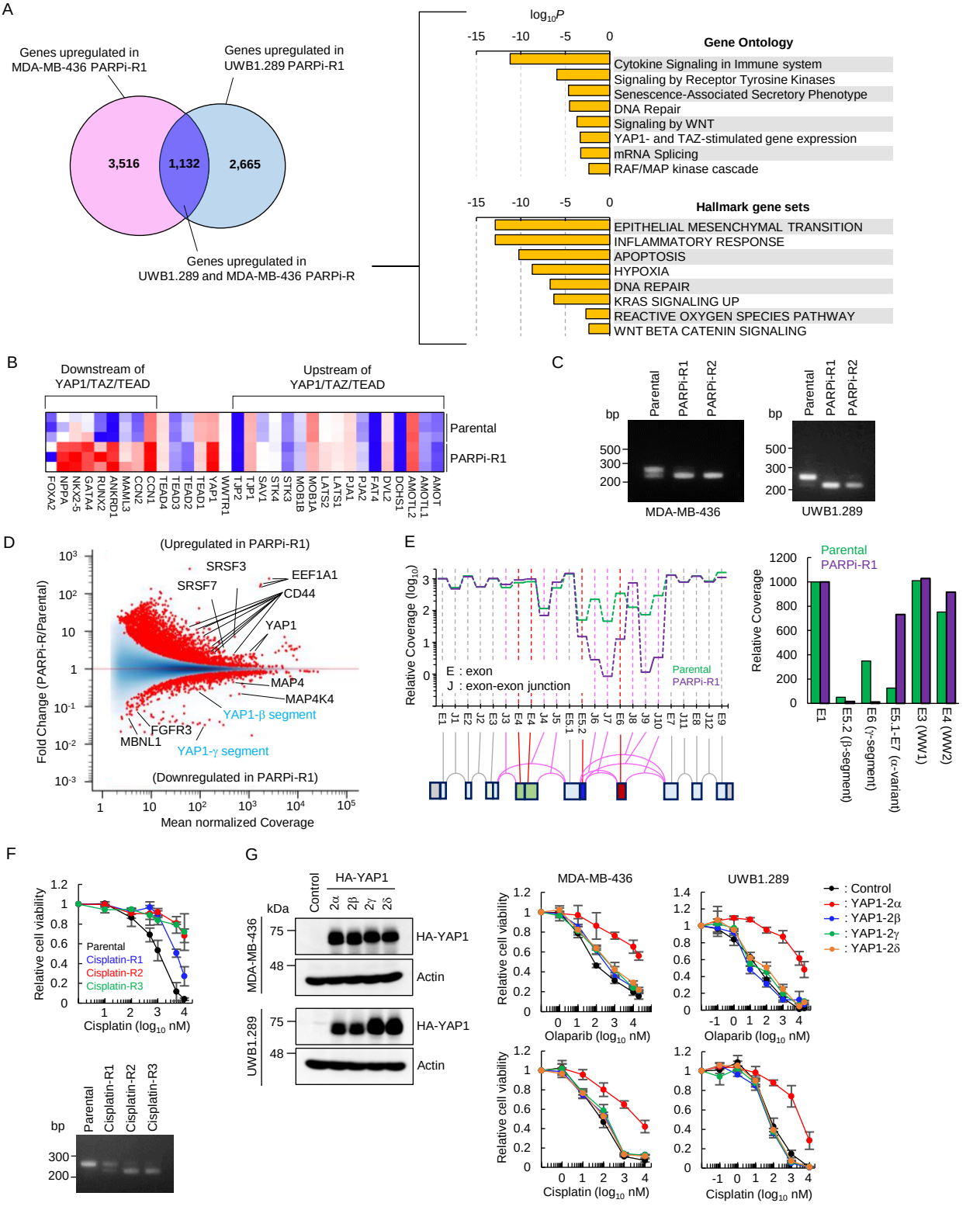
A
Genes upregulated in MDA-MB-436 PARPi-R1
Genes upregulated in UWB1.289 PARPi-R1
3,516
1,132
2,665
Genes upregulated in UWB1.289 and MDA-MB-436 PARPi-R
log10P
Gene Ontology
Cytokine Signaling in Immune system
Signaling by Receptor Tyrosine Kinases
Senescence-Associated Secretory Phenotype
DNA Repair
Signaling by WNT
YAP1- and TAZ-stimulated gene expression
mRNA Splicing
RAF/MAP kinase cascade
Hallmark gene sets
EPITHELIAL MESENCHYMAL TRANSITION
INFLAMMATORY RESPONSE
APOPTOSIS
HYPOXIA
DNA REPAIR
KRAS SIGNALING UP
REACTIVE OXYGEN SPECIES PATHWAY
WNT BETA CATENIN SIGNALING
B
Downstream of YAP1/TAZ/TEAD
Upstream of YAP1/TAZ/TEAD
Parental
PARPi-R1
FOXA2 NPPA NKX2-5 GATA4 RUNX2 ANKRD1 MAML3 CCN2 CCN1 TEAD4 TEAD3 TEAD2 TEAD1 YAP1 WWTR1 TJP2 TJP1 SAV1 STK4 STK3 MOB1B MOB1A LATS2 LATS1 PJA1 PJA2 FAT4 DVL2 DCHS1 AMOTL2 AMOTL1 AMOT
C
Parental
PARPi-R1
PARPi-R2
bp
500
300
200
MDA-MB-436
UWB1.289
D
(Upregulated in PARPi-R1)
SRSF3
SRSF7
EEF1A1
CD44
YAP1
MAP4
MAP4K4
YAP1-β segment
FGFR3
MBNL1
YAP1-γ segment
(Downregulated in PARPi-R1)
Fold Change (PARPi-R/Parental)
Mean normalized Coverage
E
Relative Coverage (log10)
E : exon
J : exon-exon junction
Parental
PARPi-R1
E1 J1 E2 J2 E3 J3 E4 E4 J4 J5 E5.1 E5.2 J6 J7 E6 J8 J9 J10 E7 J11 E8 J12 E9
Relative Coverage
E1
E5.2 (β-segment)
E6 (γ-segment)
E5.1-E7 (α-variant)
E3 (WW1)
E4 (WW2)
F
Relative cell viability
Parental
Cisplatin-R1
Cisplatin-R2
Cisplatin-R3
Cisplatin (log10 nM)
Cisplatin-R1
Cisplatin-R2
Cisplatin-R3
G
kDa
Control
HA-YAP1
2α
2β
2γ
2δ
MDA-MB-436
UWB1.289
75
48
HA-YAP1
Actin
MDA-MB-436
UWB1.289
: Control
: YAP1-2α
: YAP1-2β
: YAP1-2γ
: YAP1-2δ
Olaparib (log10 nM)
Cisplatin (log10 nM)

Figure 2.

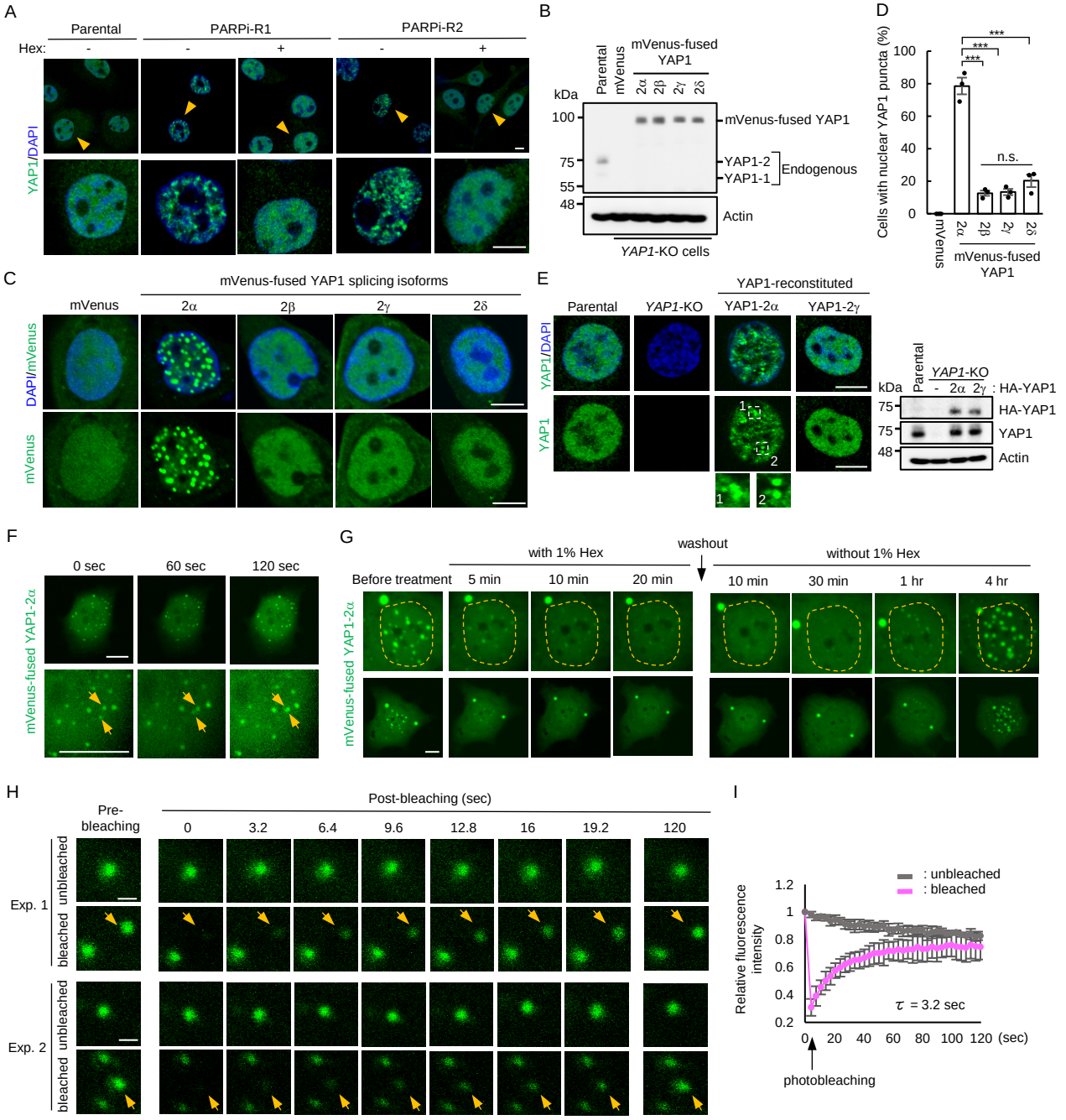
A
Parental
PARPi-R1
PARPi-R2
Hex:
YAP1/DAPI
B
Parental
mVenus
mVenus-fused YAP1
2α 2β 2γ 2δ
kDa
100
75
55
48
mVenus-fused YAP1
YAP1-2
YAP1-1
Endogenous
Actin
YAP1-KO cells
D
Cells with nuclear YAP1 puncta (%)
100
80
60
40
20
0
***
n.s.
mVenus
2α 2β 2γ 2δ
mVenus-fused YAP1
C
mVenus-fused YAP1 splicing isoforms
mVenus
2α 2β 2γ 2δ
DAPI/mVenus
mVenus
E
YAP1-reconstituted
Parental
YAP1-KO
YAP1-2α
YAP1-2γ
YAP1/DAPI
YAP1
Parental
YAP1-KO
- 2α 2γ : HA-YAP1
HA-YAP1
YAP1
Actin
F
0 sec
60 sec
120 sec
mVenus-fused YAP1-2α
G
with 1% Hex
washout
without 1% Hex
Before treatment
5 min
10 min
20 min
10 min
30 min
1 hr
4 hr
mVenus-fused YAP1-2α
H
Pre-bleaching
Post-bleaching (sec)
0
3.2
6.4
9.6
12.8
16
19.2
120
Exp. 1
Exp. 2
unbleached
bleached
I
: unbleached
: bleached
Relative fluorescence intensity
1.2
1
0.8
0.6
0.4
0.2
τ = 3.2 sec
0 20 40 60 80 100 120 (sec)
photobleaching

Figure 3.

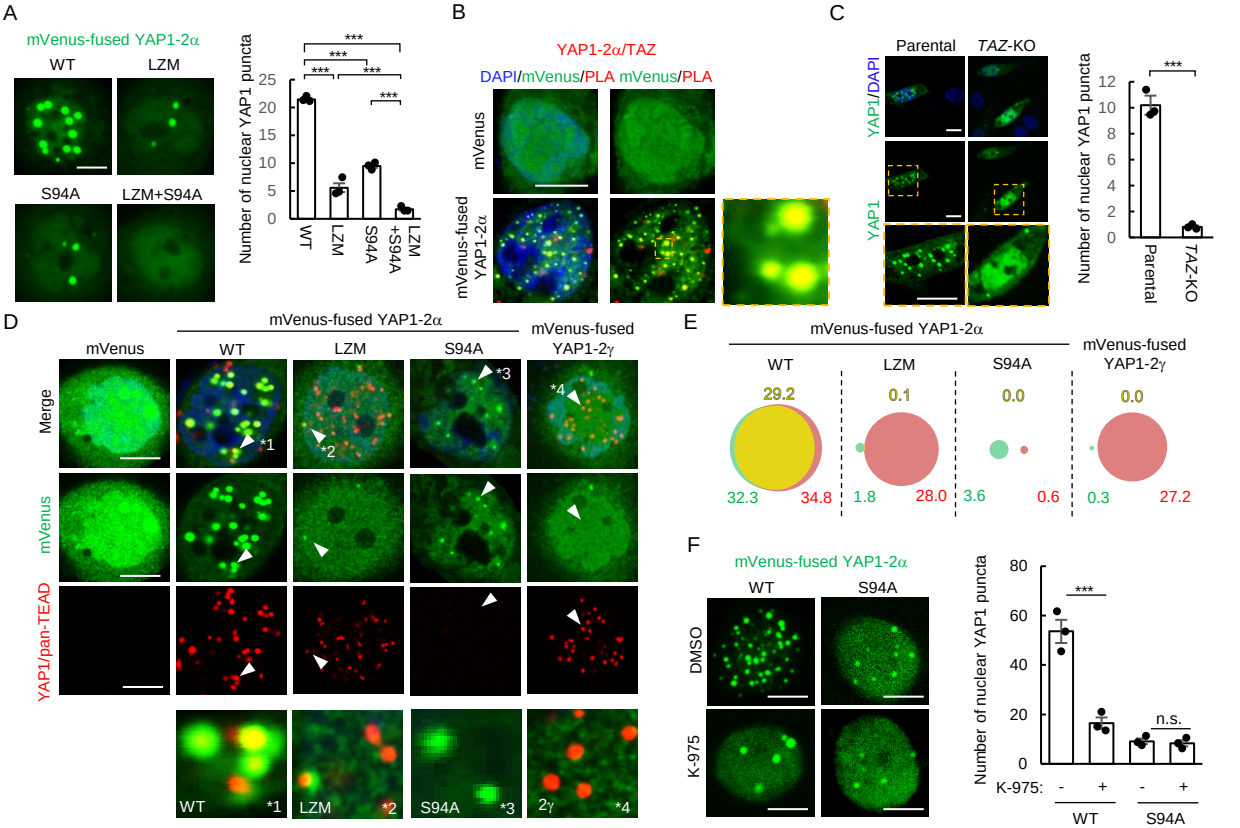
A
mVenus-fused YAP1-2α
WT
LZM
S94A
LZM+S94A
Number of nuclear YAP1 puncta
25
20
15
10
5
0
***
WT
LZM
S94A
LZM +S94A
B
YAP1-2α/TAZ
DAPI/mVenus/PLA mVenus/PLA
mVenus
mVenus-fused YAP1-2α
C
Parental
TAZ-KO
YAP1/DAPI
YAP1
Number of nuclear YAP1 puncta
12
10
8
6
4
2
0
Parental
TAZ-KO
D
mVenus-fused YAP1-2α
mVenus
WT
LZM
S94A
mVenus-fused YAP1-2γ
Merge
mVenus
YAP1/pan-TEAD
*1
*2
*3
*4
2γ
E
mVenus-fused YAP1-2α
WT
LZM
S94A
mVenus-fused YAP1-2γ
29.2
32.3
34.8
0.1
1.8
28.0
0.0
3.6
0.6
0.0
0.3
27.2
F
mVenus-fused YAP1-2α
WT
S94A
DMSO
K-975
Number of nuclear YAP1 puncta
80
60
40
20
0
***
n.s.
K-975:
-
+
-
+
WT
S94A

Figure 4.

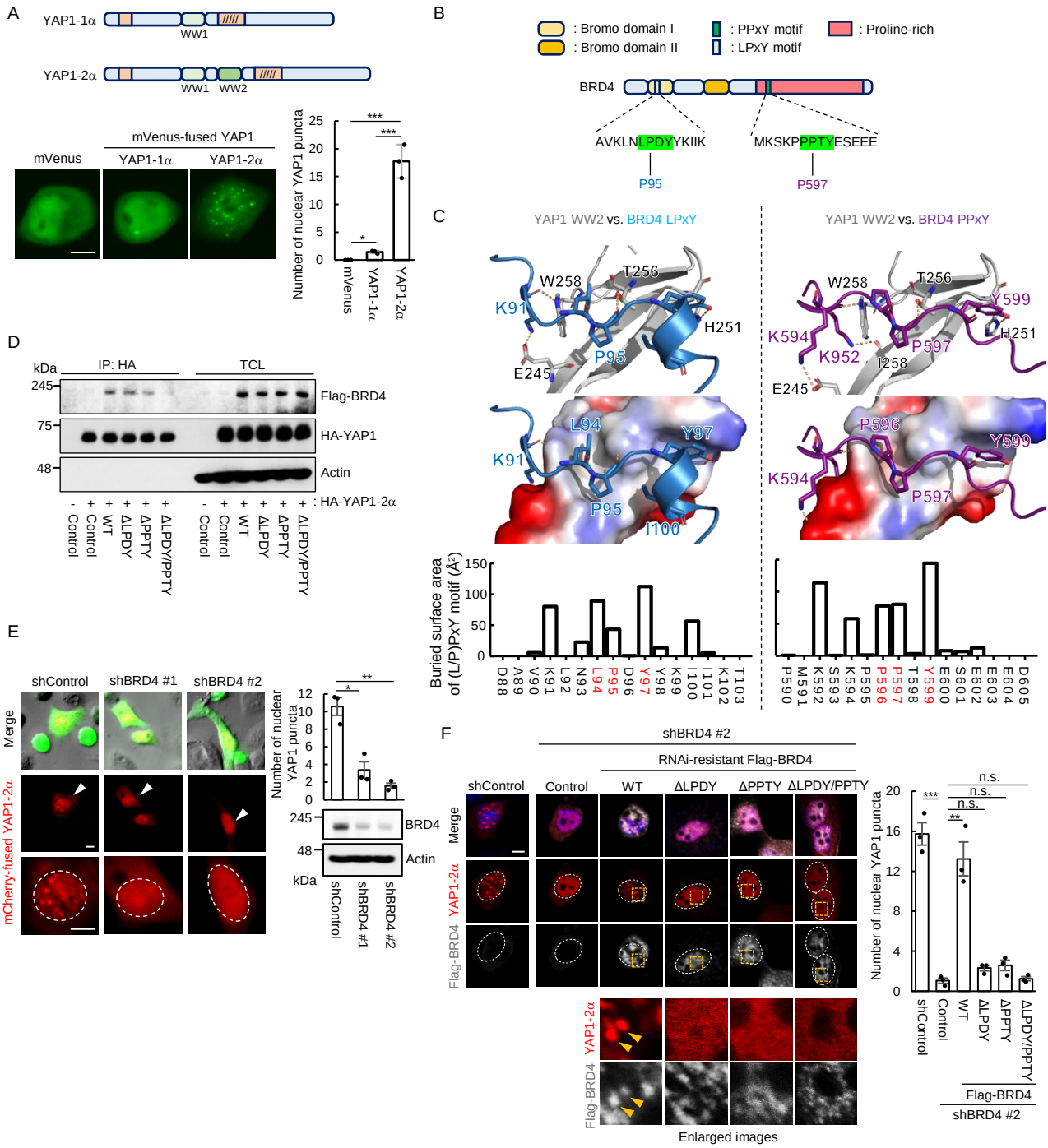
A
YAP1-1α
WW1
YAP1-2α
WW1 WW2
mVenus-fused YAP1
mVenus
YAP1-1α
YAP1-2α
Number of nuclear YAP1 puncta
mVenus
YAP1-1α
YAP1-2α
B
: Bromo domain I
: Bromo domain II
: PPxY motif
: LPxY motif
: Proline-rich
BRD4
AVKLNLPDYYKIIK
MKSKPPPTYESEEE
P95
P597
C
YAP1 WW2 vs. BRD4 LPxY
YAP1 WW2 vs. BRD4 PPxY
W258
T256
K91
H251
P95
E245
L94
Y97
I100
Y599
K594
K952
P597
I258
P596
Buried surface area of (L/P)PxY motif (Å²)
D
kDa
IP: HA
TCL
Flag-BRD4
HA-YAP1
Actin
: HA-YAP1-2α
Control
WT
ΔLPDY
ΔPPTY
ΔLPDY/PPTY
E
shControl
shBRD4 #1
shBRD4 #2
Merge
mCherry-fused YAP1-2α
Number of nuclear YAP1 puncta
BRD4
Actin
F
shBRD4 #2
RNAi-resistant Flag-BRD4
shControl
Control
WT
ΔLPDY
ΔPPTY
ΔLPDY/PPTY
Merge
YAP1-2α
Flag-BRD4
Enlarged images
n.s.

Figure 5.

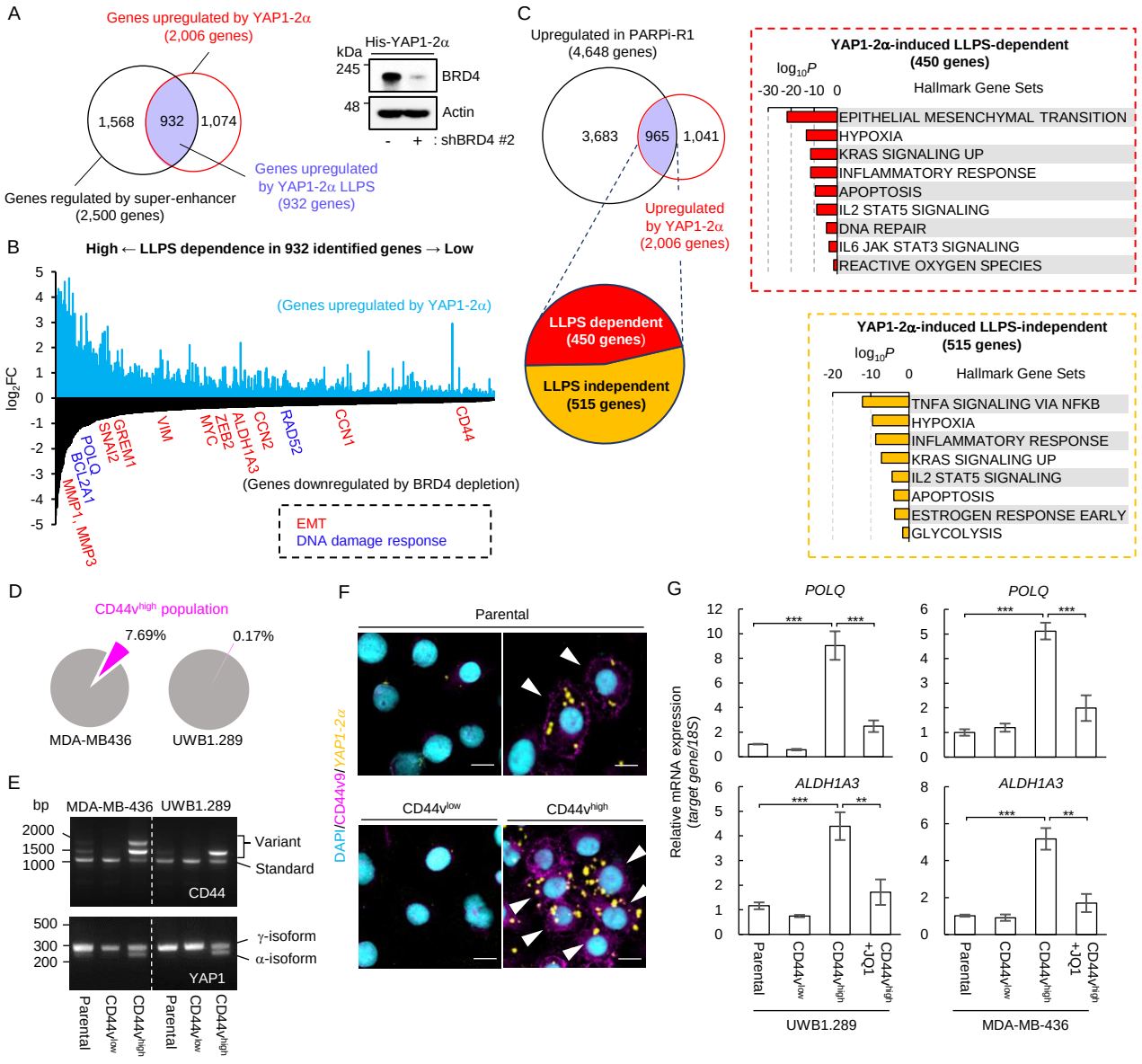
A
Genes upregulated by YAP1-2α (2,006 genes)
1,568
932
1,074
Genes regulated by super-enhancer (2,500 genes)
Genes upregulated by YAP1-2α LLPS (932 genes)
His-YAP1-2α
kDa
245
48
BRD4
Actin
- + : shBRD4 #2
B
High ← LLPS dependence in 932 identified genes → Low
(Genes upregulated by YAP1-2α)
log2FC
GREM1
SNAI2
VIM
MYC
ZEB2
ALDH1A3
CCN2
RAD52
CCN1
CD44
POLQ
BCL2A1
MMP1, MMP3
(Genes downregulated by BRD4 depletion)
EMT
DNA damage response
C
Upregulated in PARPi-R1 (4,648 genes)
3,683
965
1,041
Upregulated by YAP1-2α (2,006 genes)
LLPS dependent (450 genes)
LLPS independent (515 genes)
YAP1-2α-induced LLPS-dependent (450 genes)
log10P
Hallmark Gene Sets
EPITHELIAL MESENCHYMAL TRANSITION
HYPOXIA
KRAS SIGNALING UP
INFLAMMATORY RESPONSE
APOPTOSIS
IL2 STAT5 SIGNALING
DNA REPAIR
IL6 JAK STAT3 SIGNALING
REACTIVE OXYGEN SPECIES
YAP1-2α-induced LLPS-independent (515 genes)
TNFA SIGNALING VIA NFKB
HYPOXIA
INFLAMMATORY RESPONSE
KRAS SIGNALING UP
IL2 STAT5 SIGNALING
APOPTOSIS
ESTROGEN RESPONSE EARLY
GLYCOLYSIS
D
CD44v^high population
7.69%
0.17%
MDA-MB436
UWB1.289
E
bp
MDA-MB-436
UWB1.289
Variant
Standard
CD44
γ-isoform
α-isoform
YAP1
Parental
CD44v^low
CD44v^high
F
Parental
DAPI/CD44v9/YAP1-2α
CD44v^low
CD44v^high
G
POLQ
ALDH1A3
Relative mRNA expression (target gene/18S)
+JQ1
UWB1.289
MDA-MB-436

Figure 6.

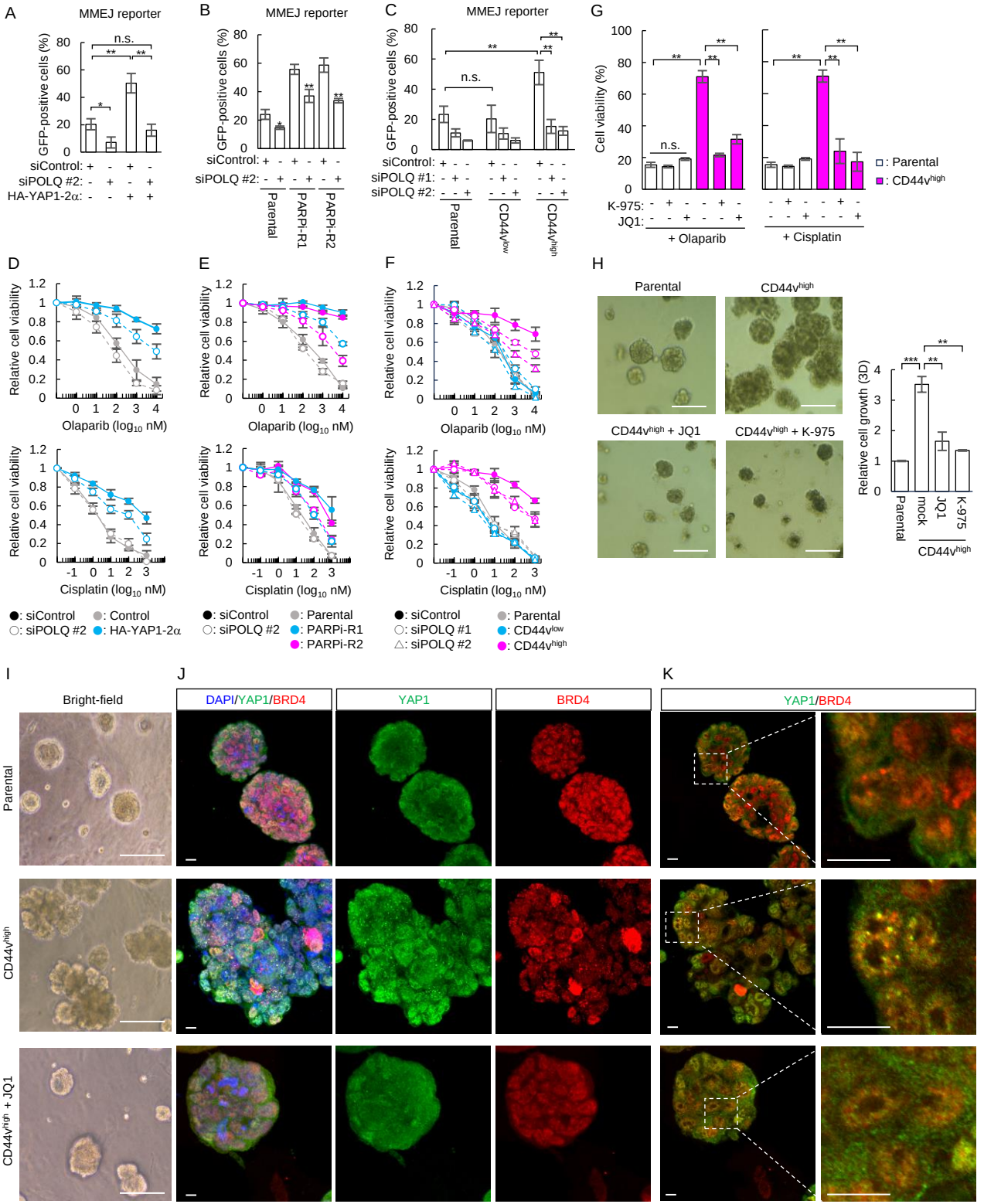
A
MMEJ reporter
GFP-positive cells (%)
n.s.
siControl:
siPOLQ #2:
HA-YAP1-2α:
B
MMEJ reporter
GFP-positive cells (%)
siControl:
siPOLQ #2:
Parental
PARPi-R1
PARPi-R2
C
MMEJ reporter
GFP-positive cells (%)
siControl:
siPOLQ #1:
siPOLQ #2:
Parental
CD44v^low
CD44v^high
G
Cell viability (%)
n.s.
K-975:
JQ1:
+ Olaparib
+ Cisplatin
□: Parental
■: CD44v^high
D
Relative cell viability
Olaparib (log10 nM)
Cisplatin (log10 nM)
●: siControl
○: siPOLQ #2
●: Control
●: HA-YAP1-2α
E
Relative cell viability
Olaparib (log10 nM)
Cisplatin (log10 nM)
●: siControl
○: siPOLQ #2
●: Parental
●: PARPi-R1
●: PARPi-R2
F
Relative cell viability
Olaparib (log10 nM)
Cisplatin (log10 nM)
●: siControl
○: siPOLQ #1
△: siPOLQ #2
●: Parental
●: CD44v^low
●: CD44v^high
H
Parental
CD44v^high
CD44v^high + JQ1
CD44v^high + K-975
Relative cell growth (3D)
Parental
mock
JQ1
K-975
CD44v^high
I
Bright-field
Parental
CD44v^high
CD44v^high + JQ1
J
DAPI/YAP1/BRD4
YAP1
BRD4
K
YAP1/BRD4

Figure 7.

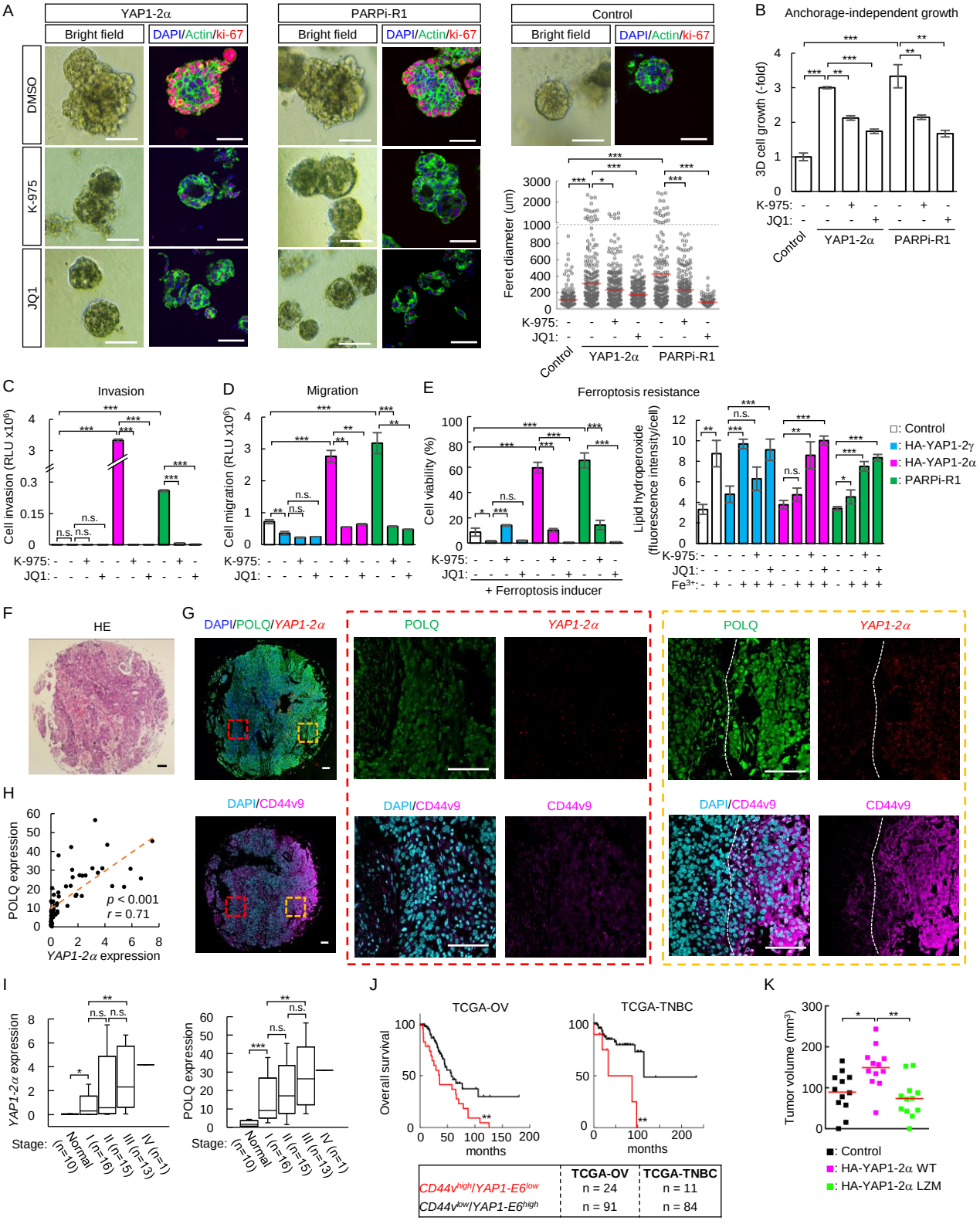
A
YAP1-2α
PARPi-R1
Control
Bright field
DAPI/Actin/ki-67
DMSO
K-975
JQ1
Feret diameter (um)
K-975:
JQ1:
B
Anchorage-independent growth
3D cell growth (-fold)
C
Invasion
Cell invasion (RLU x10^6)
D
Migration
Cell migration (RLU x10^6)
E
Ferroptosis resistance
Cell viability (%)
Lipid hydroperoxide (fluorescence intensity/cell)
+ Ferroptosis inducer
Fe3+:
□: Control
: HA-YAP1-2γ
: HA-YAP1-2α
: PARPi-R1
F
HE
G
DAPI/POLQ/YAP1-2α
POLQ
YAP1-2α
DAPI/CD44v9
CD44v9
H
POLQ expression
YAP1-2α expression
p < 0.001
r = 0.71
I
YAP1-2α expression
POLQ expression
Stage:
Normal (n=10)
I (n=16)
II (n=15)
III (n=13)
IV (n=1)
J
TCGA-OV
TCGA-TNBC
Overall survival
months
CD44v^high/YAP1-E6^low
CD44v^low/YAP1-E6^high
TCGA-OV
TCGA-TNBC
n = 24
n = 11
n = 91
n = 84
K
Tumor volume (mm3)
: Control
: HA-YAP1-2α WT
: HA-YAP1-2α LZM

Figure S1.

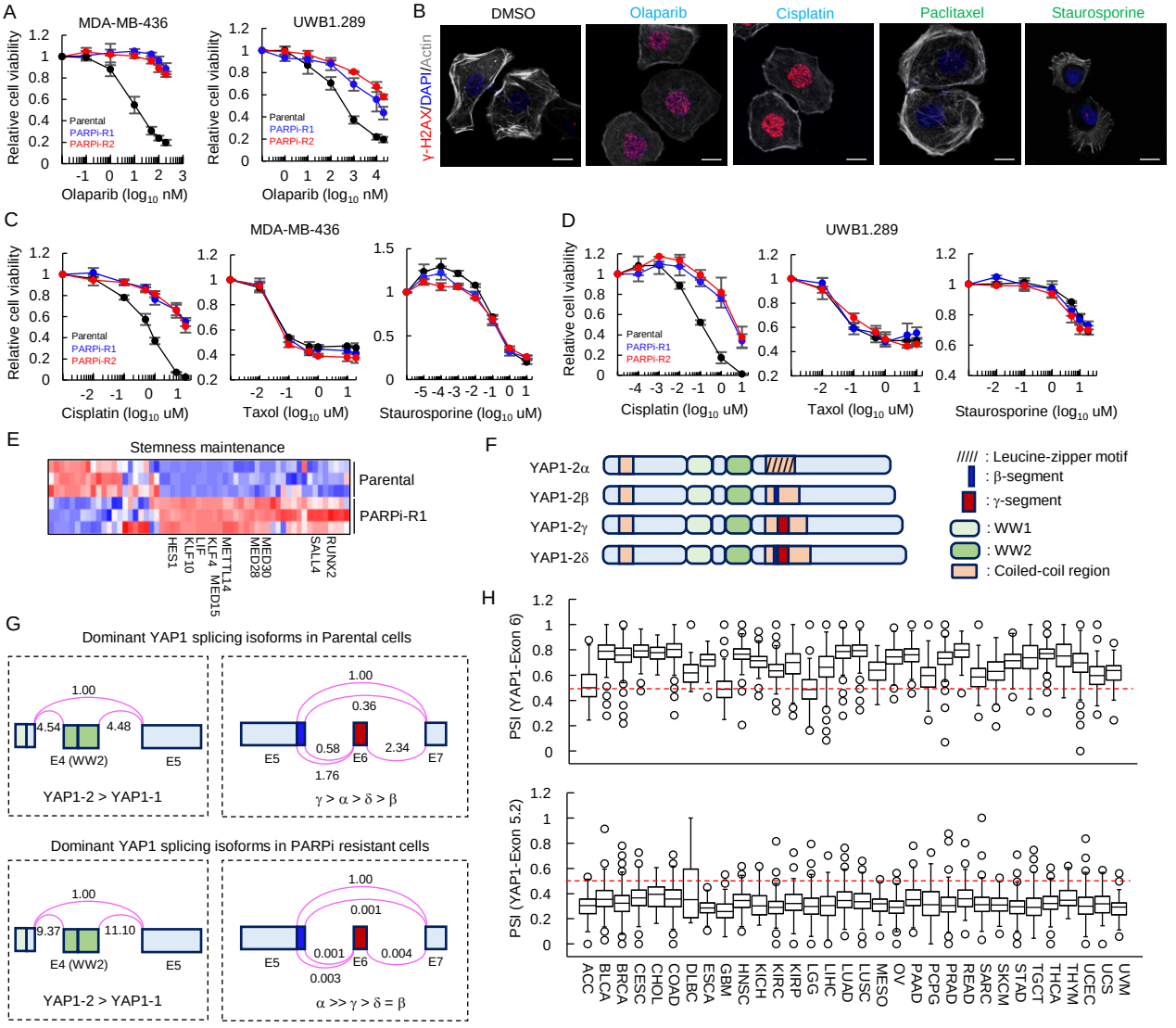

Figure S1.

(A) Related to Figure 1A. Sensitivities of *BRCA*-deficient cells (MDA-MB-436 and UWB1.289) and their PARPi-resistant descendant cells to Olaparib examined using an MTS assay.

(B) DSB induction in UWB1.289 cells treated with DNA-damaging anti-cancer drugs (Olaparib, Cisplatin) or non-DNA-damaging anti-cancer drugs (Paclitaxel, Staurosporine) visualized by an anti-γH2AX immunostaining. Scale bars indicate 10 µm.

(C and D) Sensitivities of parental and PARPi-resistant cells (C: MDA-MB-436; D: UWB1.289) to Olaparib, Cisplatin, Paclitaxel, and Staurosporine examined using MTS assay. (A, C and D) Error bars indicate mean ± SD. n=3 for each cell line.

(E) Related to Figure 1A. Heat maps showing changes in expression of the stemness-related genes. mRNA expression levels are represented as red (high) to blue (low). n=3 for each cell line.

(F) Schematic diagram of human YAP1-2 isoforms. Orange box: coiled-coil region, green box: WW1 or WW2 domain, slash bars: Leucine zipper, blue box: β-segment, red box: γ-segment.

(G) Related to Figures 1D and 1E. Relative ratios of exon skipping/inclusion with exact exon-exon junctions in *YAP1* pre-mRNAs calculated from the comprehensive alternative splicing analysis. Top: Parental MDA-MB-436 cells; bottom: PARPi-resistant cells. The relative inclusion/exclusion ratios of *YAP1* exon 4, which encodes the WW2 domain, is shown in the left panel. The relative inclusion/exclusion ratios of *YAP1* exon 6, which encodes γ-segment, and the 3'-end of *YAP1* exon 5.2, which encodes β-segment, are shown in the right panel.

(H) TCGA SpliceSeq Database (https://bioinformatics.mdanderson.org/TCGASpliceSeq/singlegene.jsp) was used to analyze the involvement of the *YAP1 β-segment* (exon 5.2, bottom) or *γ-segment* (exon 6, top) in various cancer cells. The Boxes include the 25th–75th percentiles with bars indicating medians. PSI: percent spliced-in. Dashed lines in red indicate fifty percent inclusion of the indicated exons in cancer tissue.

Figure S2.

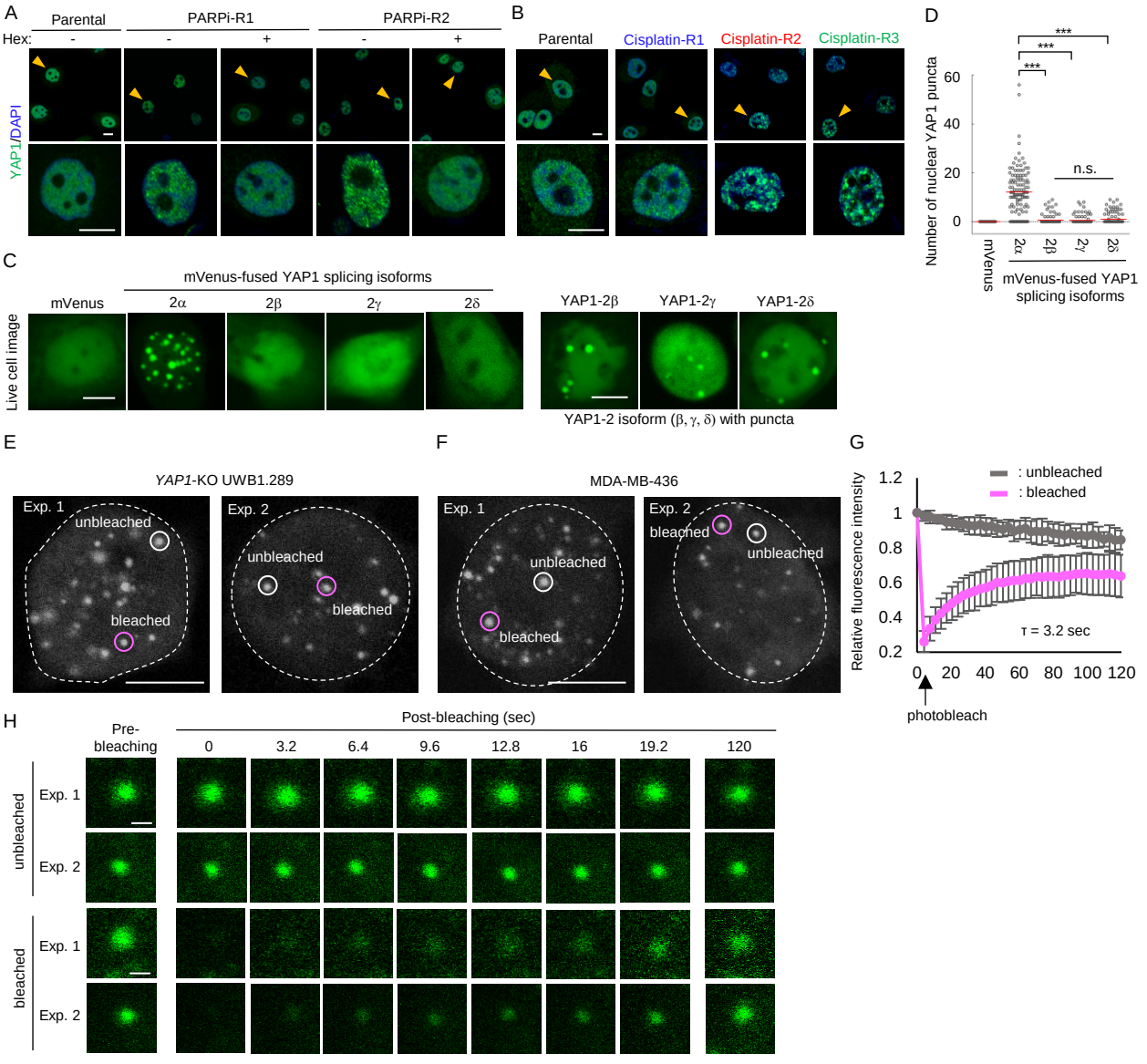

Figure S2.
(A and B) Endogenous YAP1 was visualized as a green signal using immunofluorescence staining. Nuclei were visualized using DAPI staining. The bottom panels are magnified images of the cells, indicated by the yellow arrows in the top panel. (A) Related to Figure 2A. Parental or two independent PARPi-resistant MDA-MB-436 cells (R1 and R2) treated with or without Hex. (B) Parental or three independent Cisplatin-resistant UWB1.289 cells (R1-R3) established in Figure 1F.
(C and D) Related to Figures 2C and 2D. (C) Live cell imaging analysis of *YAP1*-KO UWB1.289 cells transfected with indicated mVenus-fused YAP1 isoform plasmids. Fluorescence of mVenus was detected as a green signal. Although very rare, a few puncta-positive cells were present in cells expressing mVenus-fused YAP1-2β, γ, or δ (shown in the right three panels). (D) Number of nuclear YAP1 puncta (Fig. 2C) was calculated. ***$p < 0.001$; n.s., not significant (U test of Mann-Whitney). A total of 120 cells per group were obtained from three biological replicate experiments.
(E) Related to Figure 2H. Entire nuclear images of cells used for FRAP analysis. Two different cells were labeled as Exp. 1 and Exp. 2. White circles indicate non-photobleached puncta. The pink circles indicate photobleached puncta.
(F-H) FRAP analysis of MDA-MB-436 cells expressing mVenus-fused YAP1-2α. (F) Entire nuclear images of cells used for FRAP analysis. (G) Fluorescence intensities of puncta (photobleached; n=5, unbleached; n=5) obtained from a series of time-lapse images were analyzed. τ indicates interval of fluorescence detection. Error bars indicate mean ± SD. (H) Representative time-lapse images. Scale bars indicate 1 μm. (A, B, C, E and F) Scale bars indicate 10 μm.

Figure S3.

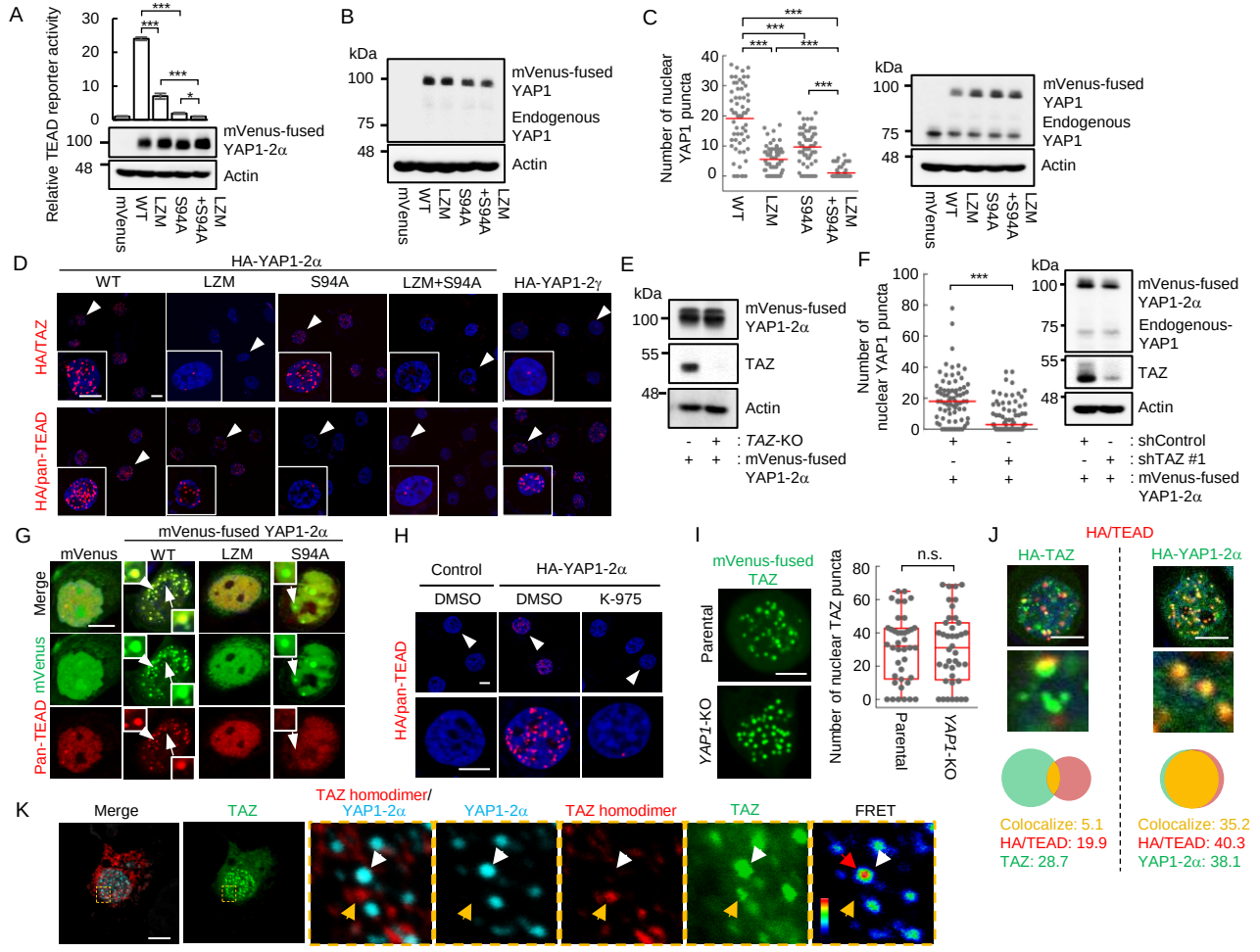

Figure S3.
(A) TEAD reporter assay of YAP1-2α mutants in *YAP1*-KO UWB1.289 cells (top panel). Error bars indicate the mean ± SD, n=3. Expression of the YAP1-2α mutant proteins (bottom panel). (B) Related to Figure 3A. The expression of the indicated proteins in *YAP1*-KO UWB1.289 cells was confirmed by immunoblotting. (C) The nuclear puncta formation in MDA-MB-436 cells expressing mVenus-fused YAP1-2α mutants. The number of YAP1 puncta in the nucleus (left). Protein expression shown by immunoblotting (right). (D) Interaction of YAP1-2α with endogenous TAZ (top) or TEAD (bottom) in UWB1.289 cells was visualized as PL spots (red) using PLA. The nuclei indicated by white arrows are magnified. (E) Related to Figure 3C. mVenus-fused YAP1-2α expression in *TAZ*-KO MDA-MB-436 cells were confirmed by immunoblotting. (F) UWB1.289 cells stably expressing shRNA targeting *TAZ* mRNA were transfected with an mVenus-fused YAP1-2α vector. Number of YAP1-2α puncta in the nucleus (left). Confirmation of TAZ knockdown and mVenus-fused YAP1-2α expression by immunoblotting (right). (G) Related to Figure 3D. Co-localization of YAP1-2α-induced puncta with endogenous TEAD in UWB1.289 cells was shown by immunofluorescence staining. (H) Related to Figure 3F. Inhibition of the physical interaction between HA-YAP1-2α and endogenous TEAD by K-975 in UWB1.289 cells was detected using PLA. (I) Effect of *YAP1* knockout on TAZ/TAZ LLPS in UWB1.289 cells. TAZ/TAZ LLPS (left). Number of nuclear TAZ puncta in Parental or *YAP1*-KO cells (right). Boxes include 25th–75th percentiles with bars indicating medians. n=40 cells for each group. (J) Interaction of YAP1-2α or TAZ with TEAD in UWB1.289 cells was visualized using PLA following immunofluorescence staining (top). Co-localization of PL spots and YAP1-2α- or TAZ puncta (bottom). Green circle: number of YAP1-2α- or TAZ puncta, Red circle: number of nuclear PL spots, Yellow circle: number of colocalized spots. n=10 nuclei. (K) UWB1.289 cells were co-transfected with mSECFP-fused YAP1-2α, mVenus-fused HA-TAZ, and Flag-TAZ and analyzed by combined FRET and PLA to detect YAP1-2α/TAZ heterodimers and TAZ/TAZ homodimers in YAP1-2α or TAZ/TAZ puncta. TAZ homodimer was visualized using PLA (red). YAP1-2α/TAZ heterodimer was detected by SECFP/Venus FRET. White arrows indicate YAP1-2α/TAZ LLPS puncta, yellow arrows indicate TAZ/TAZ LLPS puncta. All scale bars represent 10 μm.
(A, C, F and I) ***$p < 0.001$; *$p < 0.05$; n.s., not significant (A: Student's t test; C: Kruskal-Wallis post Bonferroni; F and I: Mann-Whitney U test). (C and F) Bars indicate medians, n=60 (C) or 75 (F) cells per group were obtained from three biological replicate experiments, respectively.

Figure S4.

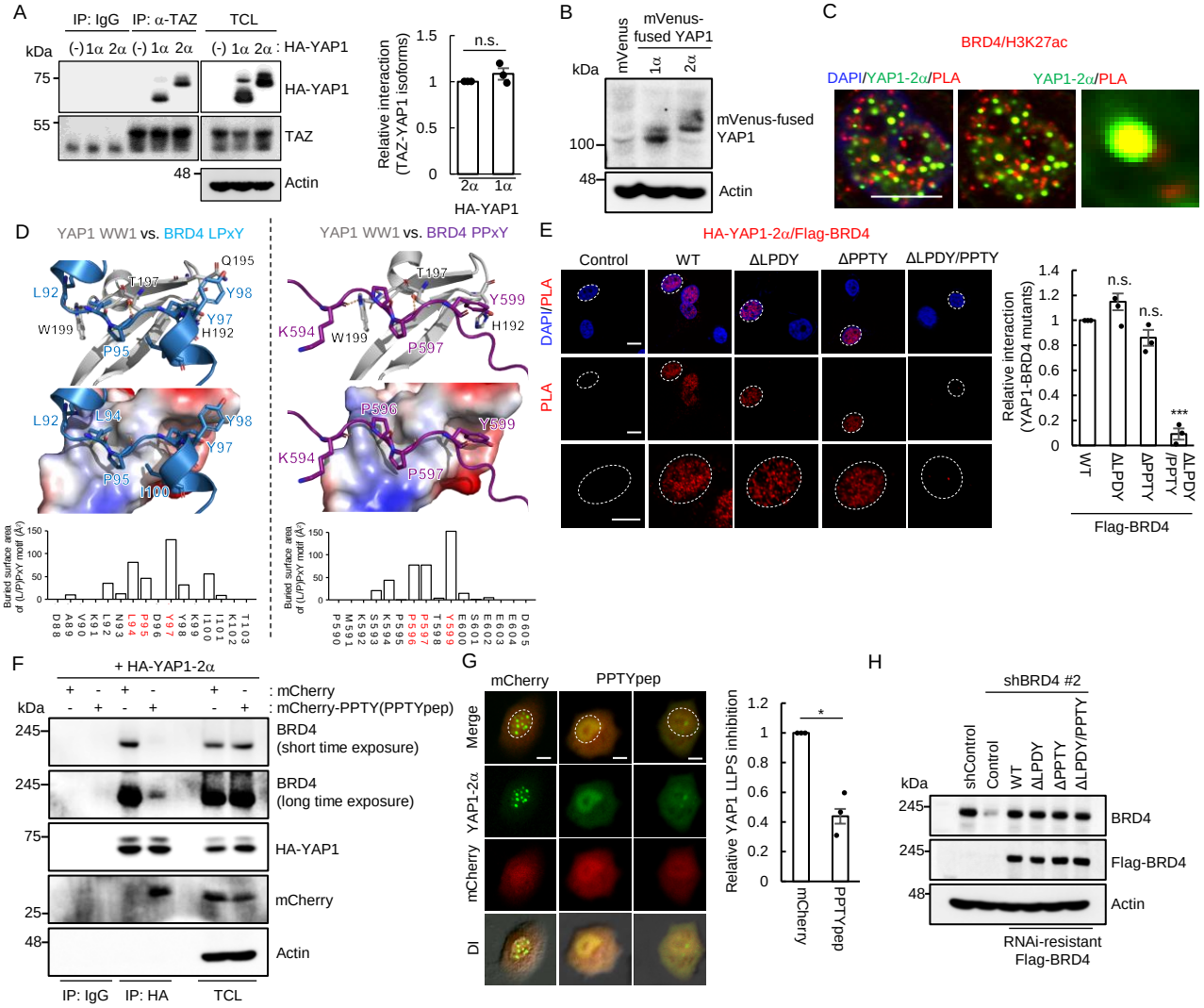

Figure S4.

(A) Interactions between TAZ and YAP1-1α or YAP1-2α in MDA-MB-436 cells were examined by an anti-HA immunoblotting analysis of the anti-TAZ immunoprecipitates. The relative interaction between YAP1-1α and TAZ was calculated by defining YAP1-2α intensity per TAZ intensity in the IP sample as one (right)

(B) Related to Figure 4A. Expression of mVenus-fused YAP1-1α and YAP1-2α in MDA-MB-436 cells was determined by immunoblotting.

(C) Co-localization of YAP1-2α LLPS puncta (green) with the H3K27ac/BRD4 complex (red), which is known as a super-enhancer marker. Complex formation between H3K27ac and BRD4 in MDA-MB-436 cells was detected by PLA.

(D) Related to Figure 4C. Predicted interaction structure of the WW1 domain of YAP1-2α with BRD4 LPxY or PPxY motif using AlphaFold2. The WW1 domain (gray), LPxY motif (blue), and PPxY motif (magenta) in each rank 1 structure are shown in the ribbon diagram (top). The vacuum electrostatic surface of the WW1 domain is represented in red (acidic) to blue (basic) (middle). The buried surface area of the LPxY and PPxY motif in the complex was estimated (bottom). The polar contacts are indicated by the orange dashed lines.

(E) Interaction between YAP1-2α and the indicated BRD4 mutant in MDA-MB-436 cells was detected as PL spots (red) using PLA (left). The relative interaction between YAP1-2α and BRD4 mutants was calculated by defining the number of YAP1-2α/wild-type BRD4 PL spots as one (right).

(F) Competitive inhibition of the YAP1-2α/BRD4 interaction using mCherry-fused PPTY peptide derived from BRD4 sequence (PPTYpep). HA-YAP1-2α-expressing MDA-MB-436 cells were transfected with the mCherry or PPTYpep vector and subjected to a sequential immunoprecipitation-immunoblotting experiment using the indicated antibodies.

(G) Inhibition of YAP1-2α puncta formation in MDA-MB-436 cells by PPTYpep, which interferes the YAP1-2α/BRD4 interaction.

(H) Related to Figure 4F. Confirmation of shBRD4 (#2)-resistant Flag-BRD4 mutants and BRD4 knockdown efficiency in MDA-MB-436 cells using immunoblotting. (A, E and G) n=3 (biological triplicate), ***$p < 0.001$; *$p < 0.05$; n.s., not significant (A: Student's t test; E: ANOVA post Bonferroni; G: Mann-Whitney U test). Error bars indicate SEM. All scale bars represent 10 μm.

Figure S5.

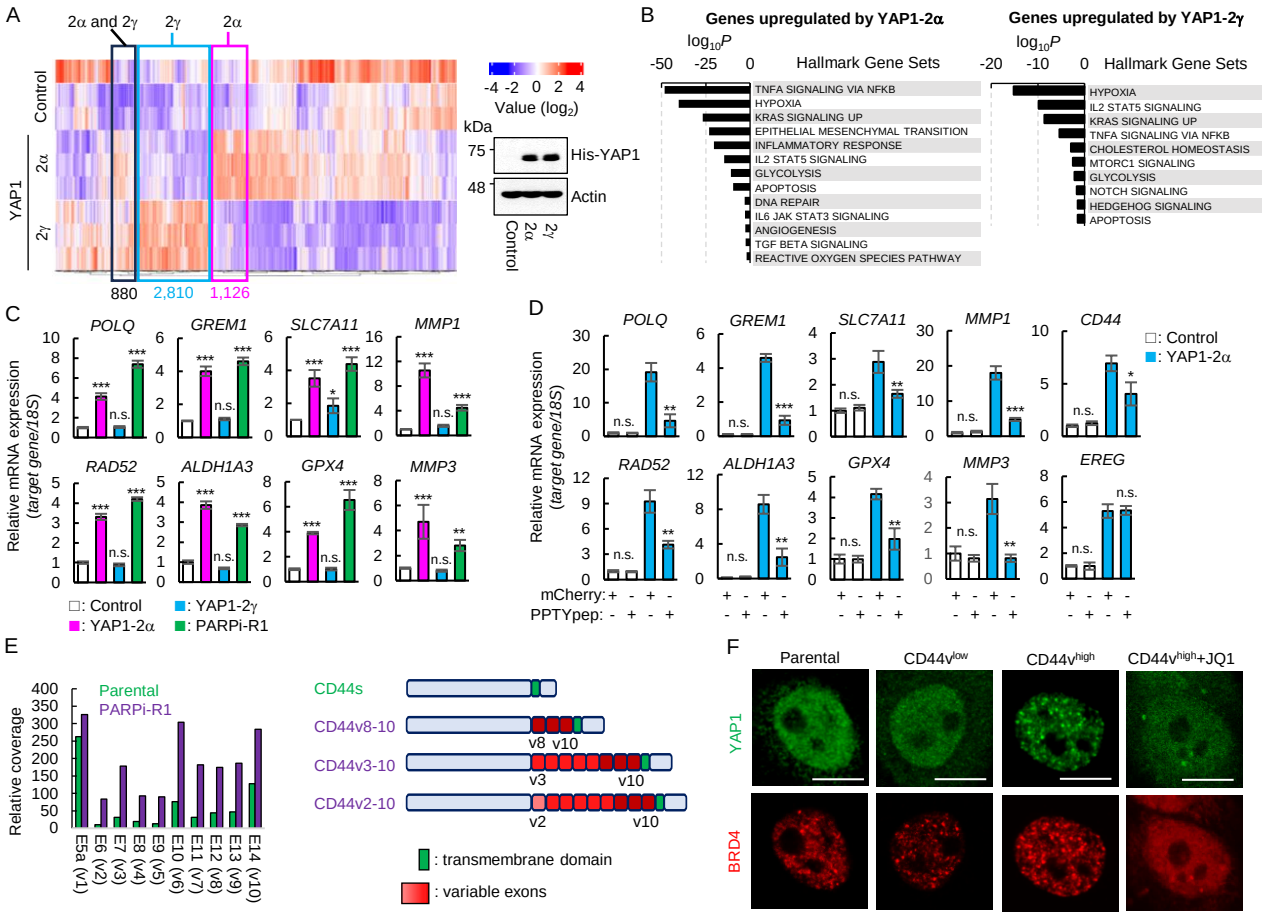

Figure S5.

(A and B) Related to Figure 5A. RNA-seq analysis of control MDA-MB-436 cells and MDA-MB-436 cells ectopically expressing YAP1-2α or YAP1-2γ (n=3 for each group). (A) Genes significantly altered by ectopic expression of YAP1-2α or YAP1-2γ ($p < 0.05$) are shown in a heatmap and the mRNA expression level is represented by red (high) to blue (low). Genes upregulated by YAP1-2α alone (Magenta box: 1,126 genes), YAP1-2γ alone (Blue box: 2,810 genes) or both YAP1-2α and -2γ (Black box: 880 genes) are indicated. Ectopic expression of YAP1-2α and YAP1-2γ in MDA-MB-436 cells was confirmed by immunoblotting (right). (B) Hallmark gene sets analysis of genes upregulated by YAP1-2α (left) or YAP1-2γ (right), respectively.

(C and D) Related to Figure 5B. Validation of mRNA expression using qPCR. Representative target genes activated by the YAP1-2α super-enhancer were analyzed using qPCR. (C) Levels of mRNA expression in MDA-MB-436 cells (Control, YAP1-2α-expressing, YAP1-2γ-expressing and PARPi-R1 cells). (D) Confirmation of YAP1-2α/TAZ/TEAD super-enhancer dependence of the validated genes. YAP1-2α/TAZ/TEAD super-enhancer formation was inhibited by ectopic expression of PPTYpep (shown in Figures S4F and S4G). *EREG*, which is regulated by YAP1-2α independently of the YAP1-2α/TAZ/TEAD super-enhancer activation, was used as a negative control. *GPX4* and *SLC7A11* were also identified as YAP1-2α/TAZ/TEAD super-enhancer target genes by qPCR.

(E) Changes in *CD44* splicing isoforms observed in Figure 1D are shown as bar graphs. Relative expression of *CD44* splicing variants in parental (green) and PARPi-resistant (purple) MDA-MB-436 cells are shown (left). Schematics of standard CD44 (CD44s) and variant CD44 (CD44v) species (right).

(F) YAP1-2α puncta formation in parental, CD44v9^{high}, and CD44v^{low} UWB1.289 cells (top). Treatment with the BRD4 inhibitor JQ1 reduced BRD4 puncta, indicating successful inhibition of BRD4-mediated super-enhancer formation (compare the third and fourth columns from the left in the bottom panels). YAP1-2α LLPS puncta were observed in CD44v^{high} cells (third column from the left in top panels), which were abolished by JQ1 treatment (fourth column from the left in top panels), indicating that YAP1-2α/TAZ/TEAD super-enhancer formation was inhibited by JQ1. Scale bars represent 10 μm.

(C and D) Error bars indicate mean ± SD. ***$p < 0.001$; **$p < 0.01$; *$p < 0.05$; n.s., not significant (Student's t test). n=3 (technical triplicate).

Figure S6.

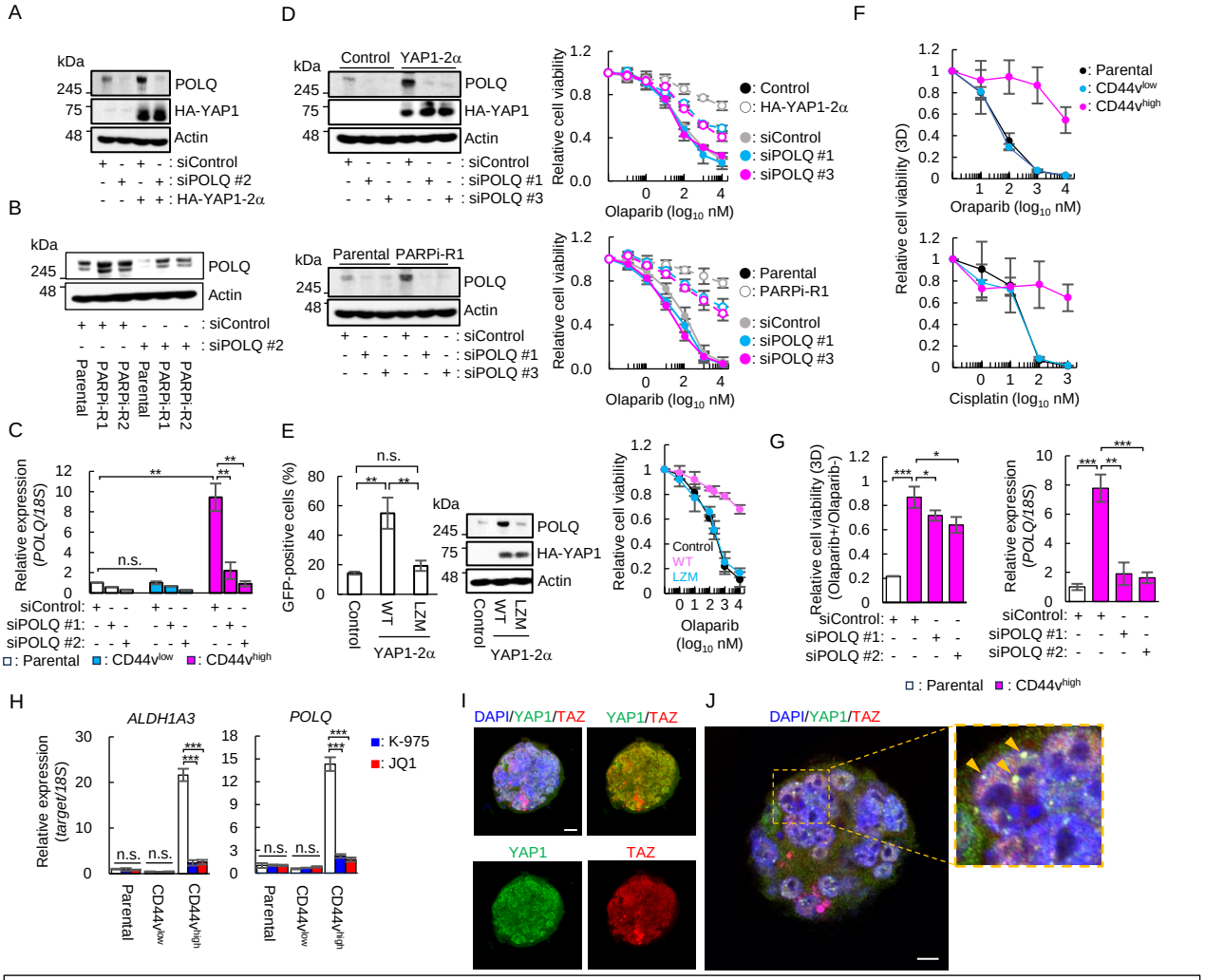

Figure S6

(A) Related to Figures 6A and 6D. The levels of the indicated proteins were examined using immunoblotting.

(B) Related to Figures 6B and 6E. The levels of the indicated proteins were examined using immunoblotting.

(C) Related to Figures 6C and 6F. The knockdown efficiencies of *POLQ* mRNA by siPOLQ #1 or siPOLQ #2 was examined by qPCR.

(D) Related to Figures 6D to 6F. To exclude off-target effects of *POLQ*-specific siRNAs, two independent siRNA sequences (siPOLQ #1 and siPOLQ #3) targeting human *POLQ* mRNA were transfected into MDA-MB-436 cells (Control, YAP1-2α-expressing and PARPi-R1 cells). The inhibition of *POLQ* expression by these siRNAs was confirmed by immunoblotting (left). Sensitivity to Olaparib was examined using the MTS assay (right).

(E) Effect of ectopic expression of wild-type (WT) or Leucine zipper-mutated (LZM) YAP1-2α on MMEJ activity (left) and PARPi sensitivity (right) in MDA-MB-436 cells.

(F) The sensitivities of parental, CD44v^{low} and CD44v^{high} UWB1.289 cells to Olaparib (left) and Cisplatin (right) were examined using 3D cell viability assay.

(G) The effect of Olaparib sensitivity on UWB1.289 spheroids (parental, CD44v^{high}) stably expressing shRNAs targeting POLQ (#1 or #2) or shControl was examined by 3D cell viability assay (left). Knockdown efficiency was evaluated using qPCR (right).

(H) Related to Figures 6G and 6H. qPCR analysis of *ALDH1A3* (left) and *POLQ* (right) mRNAs expression in Parental, CD44v9^{high} and CD44v^{low} UWB1.289 spheroids treated with K-975 or JQ1. Consistent with the sphere formation assays shown in Figure 6H, *ALDH1A3*, a stemness markers associated with accelerated spheroid formation, was increased in CD44v9^{high} cells, which was abolished by K-975 or JQ1 treatment.

(I and J) Related to Figures 6I to 6K. Co-localization of YAP1 and TAZ in YAP1-2α LLPS puncta was visualized by immunofluorescence staining with indicated antibodies. (I) Three-dimensional reconstructed images of spheroid. (J) a single-slice image of spheroid.

(C-H) Error bars indicate mean ± SD. ***p < 0.001, **p < 0.01, *p < 0.05; n.s., not significant (ANOVA post Bonferroni). n=3 (technical triplicate). (I and J) Scale bars represent 10 μm.

Figure S7.

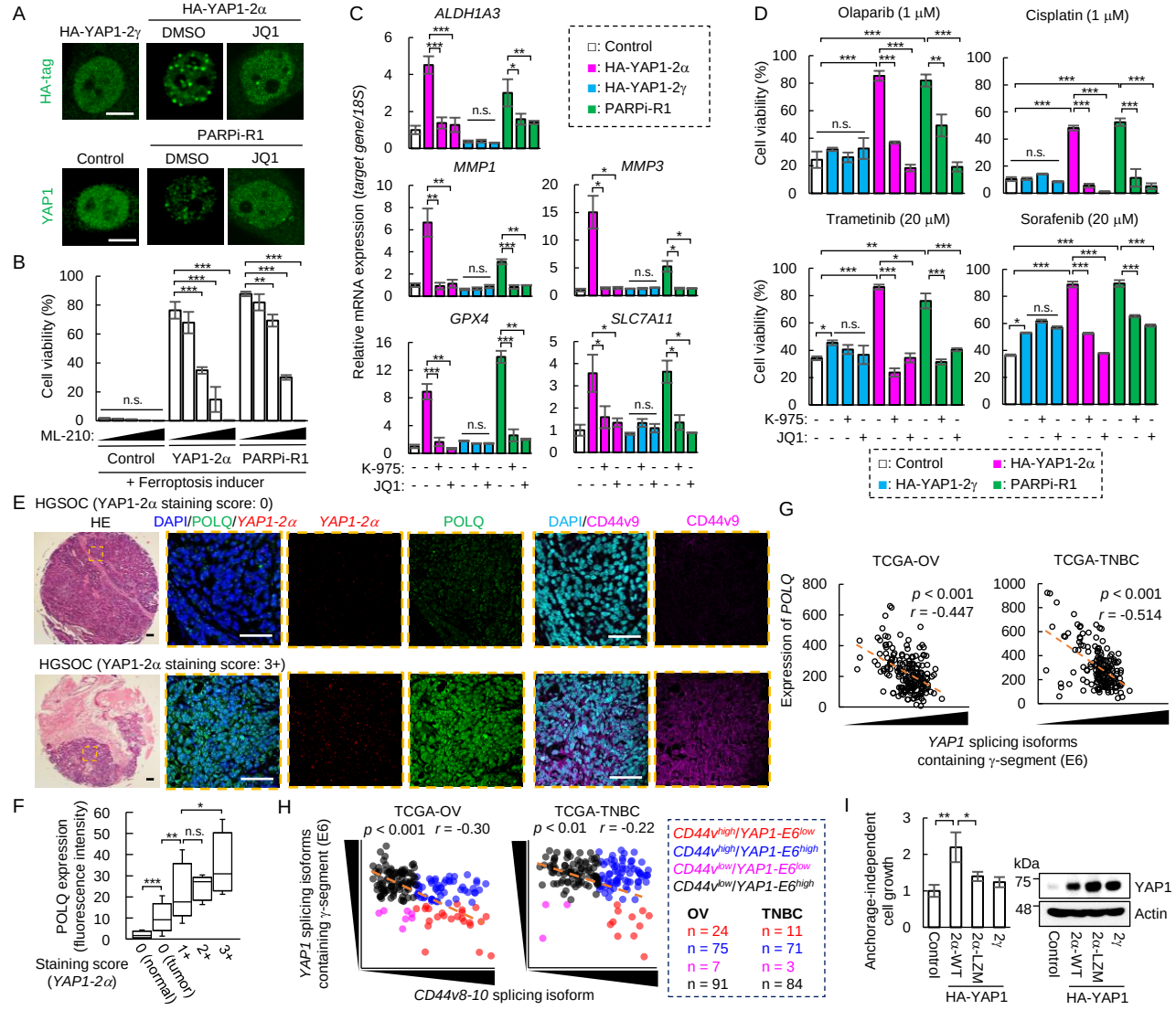

Figure S7.

(A) Related to Figures 7A-7E. Effect of JQ1 on YAP1-2α-LLPS puncta formation in ectopically YAP1-2α-expressing and PARPi-resistant UWB1.289 cells. Scale bars represent 10 μm. YAP1-2α LLPS puncta were abolished by JQ1 treatment, indicating that YAP1-2α/TAZ/TEAD super-enhancer formation was effectively inhibited by JQ1 in YAP1-2α-expressing cells or PARPi-resistant cells. (B) Related to Figure 7E. Effect of the GPX4 inhibitor ML-210 on resistance to ferroptosis in UWB1.289 cells. (C) Related to Figures 7A-7E. The expression levels of representative target genes of the YAP1-2α/TAZ/TEAD super-enhancer, which are known to be associated with the spheroids formation (*ALDH1A3*), cell invasion (*MMP1* and *MMP3*) and resistance to ferroptosis (*GPX4* and *SLC7A11*) were examined. (D) The effect of the YAP1-2α/TAZ/TEAD super-enhancer on the sensitivity of UWB1.289 cells to various anticancer drugs. (E and F) Related to Figures 7F-7I. Human tissue sections derived from patients with high-grade serous ovarian cancer were scored and classified according to the expression level of *YAP1-2α* (0, 1+, 2+, 3+). (E) HE and immunofluorescence staining images of representative tissue sections classified as *YAP1-2α* staining score 0 (top) or 3+ (bottom). CD44v9 protein (magenta), POLQ protein (green) and *YAP1-2α* mRNA (red). The yellow dashed boxes are enlarged. Scale bars represent 100 μm. (F) POLQ expression levels for each *YAP1-2α* mRNA staining score cases are shown in box-and-whisker plots. The Boxes include 25th–75th percentiles with bars indicating means and whiskers indicating range of data. (G and H) Patients with serous ovarian cancer or TNBC in the TCGA cohort were analyzed. (G) Expression correlation between *POLQ* and *YAP1-E6* is shown in scatter plots (r: Pearson's correlation coefficient). (H) Related to Figure 7J. The correlation between *YAP1-E6* and *CD44v8-10* is shown in scatter plots (r: Pearson's correlation coefficient). Black: *CD44v*^{low}/*YAP1-E6*^{high}; magenta: *CD44v*^{low}/*YAP1-E6*^{low}; blue: *CD44v*^{high}/*YAP1-E6*^{high}; red: *CD44v*^{high}/*YAP1-E6*^{low}. (I) Related to Figure 7K. Anchorage-independent growth of MKN45 cells ectopically expressing the indicated YAP1-2α mutant were examined (left). The protein expression levels of the YAP1-2α mutants were examined by immunoblotting (right).

(B, C, D, F and I) ***p < 0.001; **p < 0.01; *p < 0.05; n.s., not significant (ANOVA post Bonferroni). Except for figure S7F, n=3 (technical triplicates). All error bars indicate mean ± SD.